AN EXAMINATION OF THE CLIMATOLOGY AND ENVIRONMENTAL CHARACTERISTICS OF FLASH FLOODING FOR THE BINGHAMTON, NEW YORK COUNTY WARNING AREA

A Thesis

Presented to the Faculty of the Graduate School

of Cornell University

In Partial Fulfillment of the Requirements for the Degree of

Master of Science

by

Stephen Michael Jessup

May 2006

ABSTRACT

This study uses the publication *Storm Data* to compile a climatology of flash floods reported in the Binghamton, NY (BGM) County Warning Area (CWA) of the National Weather Service (NWS). This work reveals diurnal and seasonal trends in flash flood frequency across the CWA. Also evident is a spatial disparity in the number of flash flood reports in different portions of the CWA. In some cases, adjacent counties with similar topography reported a dissimilar number of flash floods. Because those counties reporting a strikingly smaller number of floods tended to be less populous than the neighboring counties reporting a larger number of events, a reporting bias may be to blame. Possible reporting biases aside, regional differences in the number flash flood reports across the CWA suggest that some areas are more prone to flash flooding than others.

The more significant component of the project is to analyze the environmental characteristics of flash flood events in the BGM CWA in order to refine flash flood forecasting procedures. BGM's flash flood forecasting checklist prior to this study was based on parameters and thresholds found to be significant at nearby NWS offices, rather than site-specific for BGM. Additionally, the study seeks to identify any differences between flash flood and non-flooding heavy precipitation events so as to reduce the false alarm rate. Quantitative (discriminant analysis) and qualitative (composite map) analysis has been performed to discover parameters and combinations of parameters that differ between flood and non-flood events.

The datasets are comprised of warm-season, non-tropical, meteorologically-induced flash floods, heavy precipitation events, and days in which flash flood watches were issued but flash flooding did not occur. That is, events such as dam breaks, ice jam floods, and snow melt events are excluded from the study. Events

resulting from tropical systems are excluded, as the concern is primarily to identify those conditions associated with convective warm-season events. Additionally, a data set comprised of a random year assigned to the calendar date of each flash flood event is included to represent a climatology based on the annual distribution of floods.

The results indicate that flash floods and non-floods differ most significantly in antecedent precipitation and antecedent soil moisture. Flash floods appear more likely to occur during periods of above-normal precipitation than non-floods. Wind direction at 850 mb and storm motion direction also show differences between flood and non-flood events. In particular, an easterly to southeasterly 850-mb wind or storm motion is almost always associated with flash flooding. Lastly, some parameters that had been included on the Binghamton checklist were found to be unreliable. For these parameters, the threshold values on the checklist were infrequently exceeded during flash floods, or these thresholds were more likely to generate false alarms of non-events than to warn of a flash flood.

BIOGRAPHICAL SKETCH

Steve Jessup has always been fascinated by the weather. An early obsession with snowstorms and the prospect of missing school evolved into the pursuit of a career in meteorology. Steve chose Cornell University for his undergraduate study because of its academic prowess, its natural beauty, and its matching of extracurricular activities with his interests. After earning his Bachelor's degree in Atmospheric Science, he stayed for a Master of Arts in Teaching, before deciding that public school education was not his true calling. He switched into the Master's of Science program in Atmospheric Science. His first year in the M.S. was supported by funding from the Cornell Science Inquiry Partnerships, where he was able to merge his love for teaching with his growing academic interest in atmospheric science. He has remained involved in teaching through teaching assistant positions in the Atmospheric Science department, as well as volunteer efforts with the Graduate Student School Outreach Project. This Master's project has inspired Steve to continue his education at Cornell, seeking a Ph.D. in Atmospheric Science and following up on his Master's work.

Steve has also had a long-lived interest in music, which keeps him sane when academic work becomes stressful. At one time or another, he played trumpet in practically every instrumental ensemble on campus, including the wind ensemble, jazz ensemble, marching band, pep band, symphony orchestra, chamber orchestra, pit orchestra for a musical production, and brass quintet. As a grad student, he keeps his trumpet chops intact as a full-time member of the jazz ensemble and the wind ensemble.

This thesis is dedicated to Duane and Lois Jessup, for their love and support, and to Catherine Jessup, whose love of life will always be an inspiration.

ACKNOWLEDGMENTS

Thanks to Art DeGaetano, for your advice and encouragement, and for helping me to grow as a scientist.

Thanks to Mike Evans, for your guidance and operational forecasting knowledge.

Thanks to Ashley Coles, for your hard work and careful attention to detail in assisting with the climatology portion of the project.

This project was generously supported by the Cooperative Program for Operational Meteorology, Education, and Training (COMET), as COMET Outreach Project S05-52254.

Figures 44-62 provided by the NOAA-CIRES Climate Diagnostics Center, Boulder Colorado from their Web site at http://www.cdc.noaa.gov/.

TABLE OF CONTENTS

LIST OF FIGURES

LIST OF TABLES

LIST OF ABBREVIATIONS

BGM……...……Binghamton, New York

CAPE……..Convective Available Potential Energy

CIN…….Convective Inhibition

CWA ……...……..County Warning Area

ER…….Eastern Region

JJA…….June/July/August

KSS…….…….Kuiper Skill Score

MBE……Mesobeta-scale Convective Element

MSO……..May/September/October

NARR……North American Regional Reanalysis

NCDC…….……..National Climatic Data Center

NCEP/NCAR……National Center for Environmental Prediction/National Center for Atmospheric Research

NOAA……..National Oceanic and Atmospheric Administration

NRCC……...Northeast Regional Climate Center

NWS……National Weather Service

RH……...Relative Humidity

t0…….……time closest to the flood or non-flood event

t-3…….…….……..time 3 hours before the flood or non-flood event

t-6…….…….……..time 6 hours before the flood or non-flood event

LIST OF SYMBOLS

Angle between Earth-relative and grid-relative coordinate systems……..α

Horizontal distances……..…….$\Delta x, \Delta y$

Equivalent potential temperature……..θ_e

PREFACE

The problem of flash flood forecasting has been given significant attention in the refereed literature. In general, studies of the meteorological characteristics of flash flooding take one of three forms: classification of the large-scale conditions of previous events; analysis of environmental conditions and operational forecasting methods from previous events (i.e. climatological and case studies); and theoretical formulation of the properties needed to attain and sustain heavy rainfall. The hydrological literature discusses the rainfall-runoff relationship, surface properties, and flood-routing mechanisms that contribute to flash flooding.

The seminal paper of flash-flood classification is that of Maddox et al. (1979). They classify flash flood events nationwide into four types and describe the surface and upper air signatures of each type, including the preferred locations for flood conditions. A similar discussion of different types of heavy rainfall, river flood, and flash flood events in the northeastern United States is presented in LaPenta et al. (1995). Konrad (1997) uses cluster analysis to group heavy rainfall events in the southeastern United States based on the prevailing synoptic conditions. The five groups resulting from the cluster analysis display not only distinctive synoptic weather patterns, but also differences in which predictors are most significant for each pattern. Additionally, different patterns sharing similar predictors have different typical values for these predictors.

Doswell et al. (1996) identify small- and large-scale features that are conducive to flash flooding. However, their approach is more theoretical than the previous studies. They identify long-duration heavy rainfall as the primary meteorological culprit of flash flooding, and focus on the atmospheric mechanisms

that produce such rainfall.

Many studies attempt to characterize flash floods and related heavy rainfall events by identifying and quantifying significant parameters. Funk (1991) outlines both subjective and objective techniques for forecasting heavy rainfall, using the example of a case study in the southeastern United States in May, 1987. Junker et al. (1999) discuss mesoscale convective systems that produced heavy rainfall during the central United States floods of 1993. Moore et al. (2003) examine heavy rainfall-producing warm-season elevated thunderstorms in the central United States. Harnack et al. (1999) study the lower and mid-tropospheric conditions associated with large-scale (>= 10,000 km^2) heavy rainfall events in New Jersey.

Many of these studies have defined specific forecast parameters and methodologies to improve the prediction of flash flood events. Doswell et al. (1996) state that the ability of a rain event to produce the heavy precipitation requisite for a flash flood is a function of 1) the intensity of the rainfall, and 2) the duration of the rainfall. They note that the amount of precipitation depends on the amount of moisture available and the portion of that moisture converted to precipitation. Hence, measures of water vapor concentration in the lower troposphere, its rate of ascent, and its efficiency of conversion from water vapor into liquid precipitation are all important indicators of flash flood potential. Several measures of lower- and mid-tropospheric moisture have been noted as significant in the literature: precipitable water (Funk 1991), dewpoint (Harnack et al., 1999), mixing ratio (Harnack et al., 1999; Konrad, 1997), and relative humidity (Junker et al., 1999). Warm air advection and moisture convergence at low levels is often present for these events as well (e.g. Harnack et al., 1999). The combination of lower-level wind convergence and upper-level divergence has been widely found to be a common lifting mechanism in high-precipitation or

flash-flood events (e.g. Funk, 1991; Konrad, 1997; Harnack et al., 1999). The usefulness of stability indices in predicting heavy rainfall events is questionable. Funk (1991) cites the K-index as a useful parameter. However, Konrad (1997) found that stability indices, such as convective available potential energy (CAPE) and K index, appear to be unable to distinguish between heavy and moderate precipitation events, at least for the interior southeastern U.S.

In addition to the presence of abundant moisture and a means of lifting low-level moist air, a mechanism must be in place to sustain the heavy rainfall for a long period of time in order for a flash flood to occur. Corfidi et al. (1996) developed a technique for predicting the movement of mesobeta-scale convective elements (MBEs) that are commonly responsible for mesoscale flash flood events. Slow cell movement is often a key contributor to flash floods (Doswell et al., 1996). Repeated multiple-cell movement over a region can also extend the duration of heavy precipitation, without regard to the speed of the individual cells. For example, Junker et al. (1999) found that cell training along a surface outflow boundary was the main source of a long-duration heavy rainfall.

Even with a significant source of moisture and the potential for long-duration heavy rainfall, successful prediction of a flash flood depends on anticipating the location of greatest rainfall. Bohl and Junker (1987) present a series of 1000-500 hPa thickness threshold values which are intended to anticipate the location of heaviest rainfall. Funk (1991) points out the significance of low-level jets and equivalent potential temperature (theta-e) ridges in identifying the potential location of a flash flood. Corfidi et al.'s (1996) MBE vectors provide a means of anticipating the movement of an existing MBE and, consequently, a means of anticipating the locations where its heaviest swath of rain will fall. Moore et al. (2003) confirm the usefulness of theta-e ridges and low-level jet positions as predictors of heavy rainfall

location in a study of elevated thunderstorms over the central United States.

Surface properties can play a significant role in the impact of flash floods. De Michele and Salvadori (2002) explore the dependence of flood frequency distributions produced by a hydrological model output upon the initialized antecedent soil moisture condition. In a study of flash floods in the Charlotte, North Carolina region, Smith et al. (2002) find that antecedent soil moisture is an important contributor, even in the most urbanized areas. Both Smith et al. (2000) and Creutin and Borga (2003) note that the size, slope, and shape of a basin affect the magnitude of a flash flood. Changes to the surface itself, due to urbanization, land use change, and flood control measures are also important. Ogden et al. (2000) describe the influence of engineered structures in reducing the severity of 1997 Fort Collins, Colorado flash flood.

Many of these same mechanisms produce flash flooding in the Northeastern United States. La Penta et al. (1995) characterize typical flash flood producing rainfall events in the Eastern Region (ER) of the National Weather Service (NWS) as mesoscale in nature, with substantial moisture present throughout the majority of the troposphere. However, systems with relatively dry middle or upper levels can cause a flash flood with sufficient low-level moisture and means of lifting this moisture, coupled with slow storm motion and long storm duration. Lapenta et al. (1995) also point to veering winds in the lower and middle troposphere, a diffluent 1000-500 hPa thickness pattern and a surface boundary as conducive to mesoscale heavy rainfall. In a companion article, Opitz et al. (1995) present a heavy rainfall and flooding checklist for the Philadelphia forecast office. The parameters include a lifting mechanism, such as a surface boundary or a convergence zone; a combination of high directional shear and low speed shear in the lower troposphere; preferred thickness for heavy rainfall (Bohl and Junker, 1987); precipitable water 150% of normal or greater; antecedent

precipitation; and conditions conducive to either “warm-top” or “cold-top” precipitation.

Giordano and Fritsch (1991) examine warm-season, non-tropical heavy precipitation events (which they define as a peak rainfall of at least 19 cm in a 12-h time period) in the Mid-Atlantic region. They note that heavy precipitation events are as likely to occur with northwest flow as with southwest flow, and thus could be overlooked by forecasters. They found that northwesterly flow events, without exception, had an upper-level forcing mechanism (divergence or jet maximum) nearby. In contrast, these features were present in roughly one quarter of the southwesterly flow events. For both wind directions, high dewpoints and large surface-500 hPa directional wind shear were present.

In addition to these meteorological parameters, LaPenta et al. (1995) also implicate topography as contributing to flash flood occurrence in the ER. Meteorologically, the orography of the region provides a mechanism for forced ascent, while hydrologically, steep hillsides and small basins offer the potential for rapid accumulation of runoff.

The study presented in this thesis examines the environmental conditions conducive to flash flooding in central New York and northeastern Pennsylvania. The relatively small sample size precludes a comparison of conditions for different types of events. The variables evaluated in this study are drawn from those presented in the literature and discussed above.

CHAPTER ONE

INTRODUCTION

Flash flood forecasting presents many challenges to forecasters. The complexity of the meteorological, hydrological, and topographical features that contribute to flash flooding require forecasters to be prepared when conditions are ripe for a flash flood. The National Weather Service defines a flash flood as a flood that occurs within 6 hours of the onset of the flood-producing rainfall. This short lead time, combined with the complexity inherent to the flash flood events themselves, makes it difficult to anticipate exactly where and when a flash flood will occur.

Flash floods are one of the most dangerous natural hazards, with the potential to take human lives and cause extensive property damage. Significant flash floods in recent decades include those in the Chicago area (Changnon, 1999), Fort Collins, Colorado (Weaver et al., 2000), Las Vegas, Nevada (Randerson, 1976), and Kansas (Schultz, 1984). Perhaps the most devastating flash floods in the United States, in terms of lives lost, include those in Rapid City, South Dakota (Maddox et al., 1978), and Big Thompson Canyon, Colorado (Caracena et al., 1979).

Flash floods often strike the northeastern United States as well. Perhaps the most notorious flash flood in the region is the Johnstown (Pennsylvania) flash flood of 1977 (LaPenta et al., 1995; Zhang and Fristch, 1986; ibid., 1987; Bosart and Sanders, 1981), in which heavy rainfall caused seven dam failures, resulting in 76 deaths, more than 2500 injuries, and over 200 million dollars in property damage. Part of the motivation for this study was the flash flooding within the Binghamton, NY County Warning Area during the summer of 2003, when 3 flash floods resulted in 5 deaths and over 10 million dollars in damage (NOAA, 2003)

Much of the refereed flash flood literature focuses on the central United States (e.g. Funk, 1991; Moore et al., 2003) and, specifically, on the role of mesoscale convective complexes (MCC's) in producing flash floods. Although flash floods caused by mesoscale storms are common in the northeastern United States, MCC's are rare in the region (LaPenta et al., 1995). As a result, the predictors of flash flooding and the values of those predictors vary in different parts of the country. For example, Bohl and Junker (1987) note a regional dependence in the 1000-500 hPa thickness values corresponding to the location of heaviest rainfall.

Discrepancies over which moisture variables are most useful also appear in the literature. Funk (1991) cites K index as a useful indicator of moisture for forecasting heavy rainfall in the central U.S. However, Konrad (1997) found that K index is a poor discriminator between heavy and moderate rainfall for the interior southeastern U.S. Both studies suggest that precipitable water is often a useful parameter. Konrad (1997) and Harnack et al. (1999) also found that water vapor mixing ratios at low and mid-levels tend to be higher for heavy precipitation events.

The work in this study differs in approach from other studies of flash flooding and heavy precipitation in the northeastern U.S. LaPenta et al. (1995) outline the synoptic and mesoscale features associated with both river and flash flooding. In a companion article, Opitz et al. (1995) describe some of the specific forecast tools and procedures used to forecast flooding in the region. These techniques are mostly qualitative; however, a checklist containing suggested thresholds for several parameters used at the National Weather Service Office for Philadelphia, PA is presented. Harnack et al. (1999) compare a set of events producing at least 5.1 cm (2 in.) of precipitation over an area of at least 10,000 km^2 with a climatological sample consisting of the upper-air conditions on the 5^{th}, 10^{th}, 15^{th}, 20^{th}, 25^{th}, and 30^{th} day of each month for a ten-year period (1984-93). In terms of the time and spatial scale of

interest, the study most closely related to this paper is that of Giordano and Fritsch (1991), who examined storms producing either strong tornadoes or flash flooding in the mid-Atlantic region (including New York and Pennsylvania). In contrast, this work will look to distinguish among sets of flash floods, heavy precipitation events, and flash flood watches that did not produce a flash flood over a spatial scale as small as a single county. A randomly selected sample will be included to provide a climatology.

The main objectives of this research include the following:

1. Establish a climatology of flash flood events for the BGM CWA.
2. Analyze a set of meteorological variables at the resolution of the NCEP/NCAR Regional Reanalysis (NCEP, 2005) to quantitatively identify combinations of variables that are associated with flash flooding.
3. Analyze these same variables for relevant events - including flash flood watches and instances of heavy precipitation - that did not produce flash flooding.

The ultimate goal of this project is to refine the flash flood forecasting procedures for the northeastern United States, tailoring them specifically to the conditions at NWS BGM.

CHAPTER TWO

DATA AND METHODOLOGY

Case Selection

The flash floods examined in the study were selected from the National Climatic Data Center (NCDC) Storm Events database (NOAA, 1986-2003) for the years 1986-2003. The starting date of 1986 was chosen on the basis of a comparison of events labeled as "Floods" compared with those labeled as "Flash Floods" (Figure 1). The ratio of these two types of events has been relatively stable since 1986 for events in the area of study, suggesting that the practice of reporting an event as either a "Flood" or a "Flash Flood" has remained consistent over this period of time. Prior to 1986 flash floods apparently tended to be categorized as floods owing to a step decrease in the number of flash floods reported during this time. Events labeled as "small stream" or "urban" floods were not included in this study, as their effects tend to be minor and concentrated in a very small area.

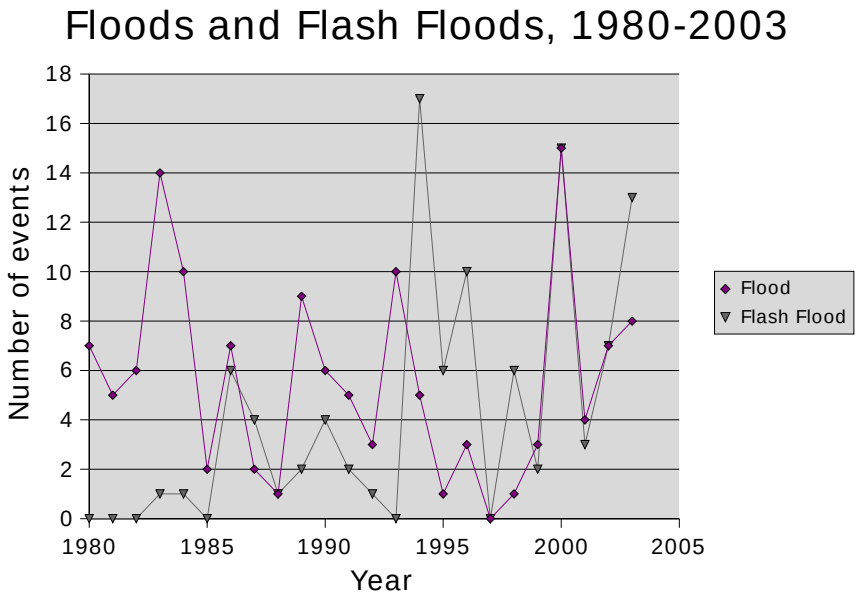

Figure 1. Flash Floods and Floods reported for the BGM CWA, 1980-20

A subset of 51 warm-season (May-October) flash flood days (hereafter "events") was selected from the 1986-2003 flash flood climatology to provide an independent, representative sample of these events. These events are listed in Table 1. The events excluded from this sample include flash floods due to the remnants of tropical systems, which do not reflect the typical environmental conditions for most flash floods that affect the region; events occurring within one week of another, which are not guaranteed to be independent on the synoptic scale; as well as dam breaks and other flash floods in which the meteorological influence was indirect. For those weeks when more than one flash flood event occurred, the representative event was selected on the basis of the number of counties affected (a multi-county event took precedence over a single-county event) and on the basis of the location of the flash floods (chosen to preserve the spatial distribution of all flash floods for the 1986-2003 period).

Some multi-county events affected several counties in the CWA over the course of several hours. For these events, the counties were blocked into groups consisting of flash flood reports separated by three hours or less. A quadrilateral bounded by the corners of the included counties was drawn to indicate the spatial extent of each grouping (Figure 2).

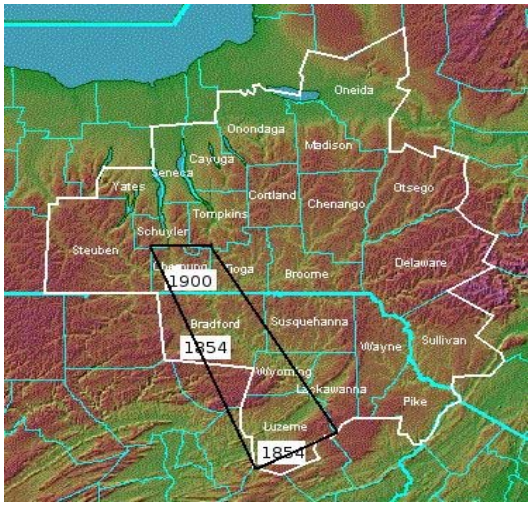

Figure 2. Example of flash flood case selection using "sufficient proximity" rule

Table 1. Flash flood events included in the NARR dataset

Date	***Time***	***County***	***Obj. C/S***	***Subj. C/S***
07/20/86	18Z	Oneida	C	C
08/06/86	21Z	Broome	C	C
08/17/86	00Z	Otsego	C	C
06/22/87	18Z	Oneida, Otsego	C	C
07/09/87	15Z	Luzerne	C	C
05/22/88	00Z	Broome	C	C
05/06/89	09Z	Otsego	C	C
06/24/89	21Z	Madison	C	C
05/17/90	18Z	Chenango	C	C
10/13/90	09Z	Bradford	S	S
10/23/90	18Z	Bradford	C	S
08/21/91	09Z	Broome, Delaware	C	S
07/31/92	12Z	Cayuga, Steuben, Yates	C	S
06/13/94	21Z	Schuyler, Steuben	C	C
06/27/94	18Z	Bradford	C	C
07/06/94	18Z	Bradford, Chemung, Pike	C	C
07/18/94	18Z	Bradford	C	C
08/18/94	06Z	Cayuga, Chemung, Cortland, Schuyler, Steuben, Tioga, Tompkins	C	S
09/27/94	03Z	Chemung, Tioga	S	C
06/27/95	03Z	Bradford	C	C
07/17/95	00Z	Delaware, Otsego	C	C
08/16/95	00Z	Cayuga, Onondaga	C	C
10/21/95	12Z	Chemung	C	C
04/30/96	15Z	Steuben, Seneca, Yates	S	C
05/10/96	21Z	Tompkins	C	C
06/08/96	21Z	Otsego	C	C
09/08/96	21Z	Pike	C	C
11/09/96	06Z	Delaware, Sullivan, Wayne	C	C
06/13/98	21Z	Bradford, Schuyler, Susquehanna	C	C
06/30/98	18Z	Broome, Sullivan	C	C
07/08/98	15Z	Broome, Chenango, Delaware	S	S
08/24/98	21Z	Onondaga	C	C
07/04/99	09Z	Delaware, Oneida, Otsego	C	C
05/13/00	18Z	Broome, Chenango, Cortland, Delaware, Madison, Oneida, Otsego, Tioga	C	C
06/13/00	21Z	Steuben	C	C
07/15/00	12Z	Luzerne	S	S
07/30/00	18Z	Wyoming	C	C
08/11/00	21Z	Sullivan	C	C

Table 1. (Continued)

Date	*Time*	*County*	*Obj. C/S*	*Subj. C/S*
09/03/00	00Z	Wayne	C	C
09/23/00	12Z	Yates	S	S
06/23/01	15Z	Broome, Chenango, Madison, Oneida, Tioga	C	S
05/28/02	18Z	Lackawanna, Luzerne, Sullivan, Wayne	C	C
06/14/02	09Z	Onondaga	S	S
06/25/02	21Z	Broome	C	C
05/02/03	00Z	Bradford	C	C
06/01/03	09Z	Lackawanna	S	S
06/14/03	00Z	Broome, Delaware	C	S
06/21/03	18Z	Bradford	C	S
07/22/03	21Z	Chemung, Schuyler, Tompkins	C	C
08/12/03	03Z	Steuben	C	C
09/04/03	03Z	Lackawanna, Sullivan, Wayne	S	C

If the combined area of those counties reporting a flash flood was greater than the combined area of those counties not reporting a flash flood within the quadrilateral box, this grouping was eligible for inclusion in the subset of events to be analyzed. All future references to “sufficient proximity” refer to this technique. The choice of which grouping of counties to select from a particular event was made such that the subset of events to be included in the study would preserve the overall spatial distribution of all flash flood events.

Three sets of non-flood events were selected for comparison. The first set establishes a climatological comparison for seasonal values. This dataset was constructed by retaining the dates and locations of the flash floods but randomly assigning a year between 1986 and 2003 that did not coincide with a flash flood or river flood to each event. All members of this "random" dataset were separated from both each other and from all flood and flash flood events reported in *Storm Data* by at least one week (seven days). The amount of precipitation was not a factor in the determination of this non-event dataset. The goal of these data was to create a

climatology of equal sample size based on the seasonal distribution of the flash flood events.

The second non-event dataset consisted of heavy precipitation events that did not result in a flash flood. These cases were selected using data from the NOAA Hourly Precipitation Dataset. A "heavy" event was defined as an hourly report of at least 2.54 cm (one inch) and a total of at least 3.8 cm (1.5 inches) in a six hour period. The time of the heavy rainfall event was recorded as that of the highest hourly amount. To assure the independence of synoptic conditions, each case in the dataset was separated from both the other cases and from all flood and flash flood events reported in *Storm Data* by at least seven days. This resulted in a dataset consisting of 36 members, which are listed in Table 2.

Table 2. Heavy precipitation events included in the NARR dataset

Date	***Time***	***County***	***Obj. C/S***	***Subj C/S***
06/16/86	21Z	Pike	C	C
09/29/86	18Z	Cayuga	C	C
05/24/87	00Z	Susquehanna	C	C
05/31/87	18Z	Sullivan	C	C
07/03/87	03Z	Luzerne	C	C
06/16/88	21Z	Wyoming	C	C
07/13/88	00Z	Luzerne	C	C
08/28/88	21Z	Tioga	C	C
10/19/88	18Z	Otsego	C	C
07/05/89	09Z	Susquehanna	C	C
08/05/89	00Z	Cayuga, Cortland	C	C
09/17/89	03Z	Pike	S	S
06/15/90	09Z	Schuyler	C	C
07/23/90	15Z	Oneida	S	S
08/13/90	21Z	Madison	C	C
08/29/90	00Z	Broome, Tioga	C	C
09/19/91	03Z	Luzerne, Sullivan	C	C
07/16/92	00Z	Pike, Bradford	C	C
09/22/92	21Z	Bradford	C	C
06/15/93	21Z	Bradford	C	C
07/15/93	00Z	Sullivan	C	C

Table 2. (Continued)

Date	*Time*	*County*	*Obj. C/S*	*Subj C/S*
07/15/93	00Z	Sullivan	C	C
09/04/93	00Z	Sullivan	C	C
07/27/95	21Z	Sullivan	C	C
08/05/95	15Z	Bradford	C	C
07/03/96	06Z	Pike	C	C
07/15/96	18Z	Oneida	C	C
08/08/96	18Z	Schuyler	C	C
08/28/96	06Z	Sullivan, Susquehanna	C	C
05/30/98	09Z	Lackawanna	C	C
07/30/99	00Z	Otsego	C	C
09/07/99	09Z	Luzerne	C	S
08/03/01	18Z	Otsego	C	C
09/25/01	06Z	Sullivan	S	S
07/23/02	21Z	Pike	C	C
09/15/02	18Z	Luzerne	C	C
09/23/03	09Z	Madison	C	C

When two or more counties within sufficient proximity fulfilled the heavy precipitation criteria on the same day, both counties were included spatially, and temporally the later time was chosen. This approach was based on the assumption that the increased saturation of the ground at the later time would more closely approximate the surface conditions at the time of a flash flood. If these counties were not within sufficient proximity of one another, the county selected was chosen to more closely approximate the spatial distribution of the flash flood events.

The third and final non-event dataset consists of 17 flash flood watches for the counties in the current BGM CWA between 1995 and 2003 that did not result in a flash flood (Table 3). Once again, each "watch" event was separated from other

watches by at least one week. However, eight of the watches in the dataset occurred within a week of a flash flood or river flood either in the same county or elsewhere in the CWA. Due to the small sample size of this dataset, these events were not removed.

Table 3. Flash flood watch events included in the NARR dataset

Date	***Time***	***County***	***Obj. C/S***	***Subj. C/S***
06/03/95	21Z	Steuben, Tompkins	C	C
08/02/95	21Z	Sullivan, Delaware	C	C
06/10/95	12Z	Sullivan	C	C
06/19/96	15Z	Luzerne	S	C
07/19/96	18Z	Delaware, Otsego	C	C
09/07/96	12Z	Susquehanna	C	S
08/21/97	00Z	Pike, Luzerne	C	S
09/11/97	15Z	Pike	C	C
06/18/98	00Z	Otsego	C	C
07/06/99	21Z	Delaware	C	C
05/19/00	06Z	Steuben	S	C
08/03/00	21Z	Susquehanna	C	C
07/26/01	12Z	Sullivan	C	C
06/12/02	18Z	Sullivan	C	C
09/27/02	03Z	Wayne	S	S
08/03/03	00Z	Steuben	C	C
09/15/03	09Z	Wayne	S	C

The Hourly Precipitation Dataset was used to resolve the spatial and temporal scales of the watches (which tend to be issued for relatively large areas and relatively long time periods) to a one- to three-county area over a six-hour time period, such that they were comparable to the flash flood events. For each watch event, the station(s) with the highest one-hour precipitation amount determine the county/counties and

time of the watch event. If two or more stations within sufficient proximity recorded similar precipitation amounts (amounts differed by less than 0.25 cm) within a three-hour time period, the counties of both stations were included in the dataset. When these conditions were met in multiple time periods for the same watch, the county grouping corresponding to later time period was chosen.

This was based on the assumption that the additional accumulated rainfall over this longer time period increases the soil moisture, making the surface conditions more similar those of the flash flood events. Because this method was applied only when counties were in close proximity to one another, this approach does not suffer from biasing the dataset to downstream locations, with respect to storm motion. Finally, in the instances when more than one flash flood watch occurred within one week, the case with the greater maximum hourly precipitation total was chosen, based on the assumption that this case would more closely approximate the flash flood cases' precipitation characteristics.

The flood, heavy, and watch cases were further classified as being either convective or non-convective in nature. The distinction between convective and non-convective events was determined in two independent ways. The first was a subjective classification based on the position of the low pressure center in relation to the location of the flood. Those events that remained to the north and/or west of the low pressure center (that is, out of the warm sector) were judged to be non-convective. Convective events included those events occurring in the warm sector of an extratropical cyclone as well as those events occurring in the absence of (or far removed from) a low pressure center.

The second method of identifying convective events involved the surface-based convective available potential energy (CAPE) and Showalter Index (SI; Showalter, 1953) associated with each event. Those cases with a CAPE less than 75

J/kg at the time of the flash flood (t0) and at three hours prior to the flood (t-3), as well as a positive SI, were classified as non-convective events and removed from the discriminant analysis. The time t-3 values were included to reduce problems with the triggering of the model's convective scheme parameterization, which may have under-estimated the CAPE at t0. In general, most events classified as non-convective by the subjective classification scheme were similarly classified by the objective classification scheme. Tables 1-3 note whether each event was classified as convective or non-convective based on each technique.

Precipitation Climatology

A climatology of precipitation was constructed using the Northeast Regional Climate Center's (NRCC) database of cooperative station daily precipitation data. To assess the precipitation attributed to each event, a 48-hour total - including the day of and the day after each flash flood report - was compiled for every station in each county reporting a flash flood. Additionally, climatologies were constructed for three time periods prior to the flash flood event: 7 days, 14 days, and 30 days. This evaluated both the short-term precipitation directly associated with the flash flood event and the effect of recent rain in increasing the soil moisture and raising stream levels. The long-term climatologies also offered a means to determine whether wet periods tend to be more conducive to flash flooding than normal or dry periods.

For each flash flood, the station in each county with the highest reported 48-hour precipitation total was used to represent that county for the given flash flood event in the climatology. In some cases flash floods occurred simultaneously in several counties, with each county contributing its own station to the climatology. As a result, some cases contribute more values to the climatology than others (i.e. a ten-county event will contribute ten data points whereas a one-county event will contribute one data point). However, this approach does provide benefits. For

example, it increases the sample size such that it can show whether there is a spatial dependence in the amount of precipitation needed to produce a flash flood in different areas of the CWA.

In constructing the longer time period (7 days and longer) antecedent precipitation climatologies, the precipitation totals include the time period up to and including the day before the flash flood. Steps were taken in addition to the procedure described above to ensure that there was no overlap of flash flood events represented in the climatology. Temporal independence was assured by including only the first flash flood per time period and county. For example, if a flash flood occurred in a certain county both on 10 June 2003 and 15 June 2003, only the 10 June precipitation amount was used in the 7-day, 14-day, and 30-day climatologies. As a result, the sample size of the 7-day climatology is larger than the sample size of the 14-day climatology, which is larger than the sample size of the 30-day climatology. Also, these climatologies of different lengths are not independent from each other. The 7-day climatology is a subset of the 14-day climatology, and the 14-day climatology is a subset of the 30-day climatology.

A climatology of non-flood events was constructed to represent typical 7-day, 14-day, and 30-day precipitation amounts within the CWA. This climatology consists of the precipitation total on the same date and in the same county as the flash flood, but in those years from the period of record (1986-2003) during which that county did not report a flash flood at any time during the time period of interest. Thus, this allows a comparison between those years reporting a flash flood and those not reporting a flash flood during the same time of year and in the same location.

Environmental Conditions

The NCEP/NCAR North American Regional Reanalysis (NARR) (Mesinger et al., 2005) was used to explore the atmospheric conditions prior to the flash floods (see

Figure 3 for the domain used in this study). The NARR has a spatial resolution of 32 km and a temporal resolution of 3 hours, which allows the meteorological conditions associated with flash flood events to be resolved to the approximate location of the county in which they occurred. Each county in the CWA was defined in a quadrilateral bounded by four NARR grid points. The boundaries of each flash flood event and non-flood event were determined by the northwestern most, northeastern most, southwestern most, and southeastern most points of those counties comprising the event.

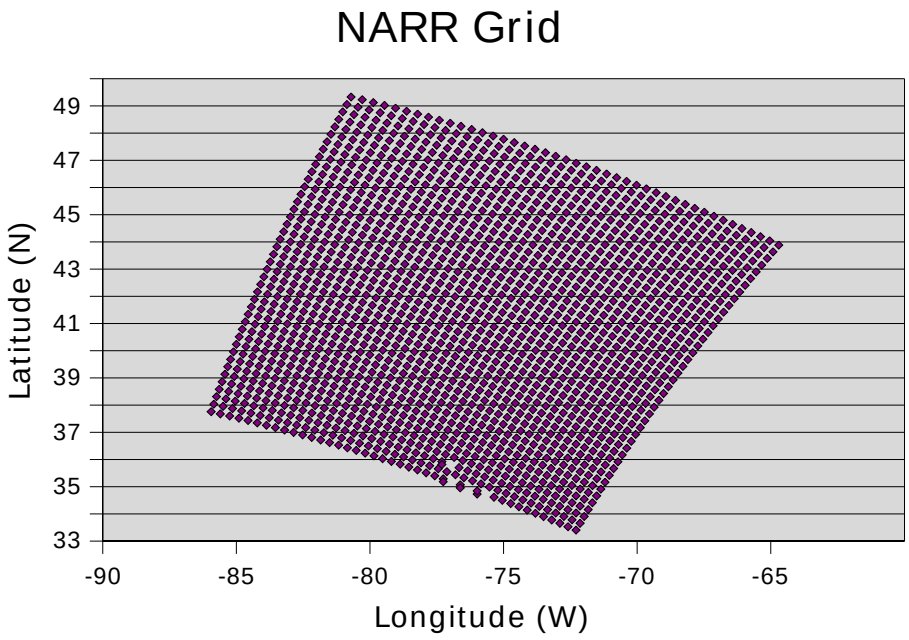

Figure 3. Domain of NARR data

Parameters of interest were averaged over this initial area at the time preceding either the reported flash flood or the heaviest hourly rainfall report. A list of these parameters can be found in Table 4. They included measures of local conditions, such as temperature, moisture, and winds, as well as synoptic conditions, such as divergence at upper and lower levels, thickness diffluence, and the presence of a ridge of equivalent potential temperature (θ_e).

The time of the flood, heavy and watch events was defined as the NARR time period preceding the reported time of the flash flood in Storm Data (flood events) or the recorded time of heaviest rainfall (heavy and watch events). Delays in reporting the flash floods may not accurately reflect the floods' true time of onset. However, the flash flood times as reported in Storm Data compared favorably with the time of peak precipitation for nearby hourly rain gauges. Thus, the timing of the flash floods is consistent with the timing of the heavy and watch events.

The NARR was evaluated for three time periods: the initial time period, just before the event (t0), and the two time periods occurring prior to this (t-3 and t-6). A backtracking technique was employed to trace the low-level inflow backwards from the t0 location for the earlier two time periods to evaluate the upstream conditions (with respect to the inflowing air) preceding the event. The 850-hPa winds at the northwest, northeast, southwest, and southeast corners of the quadrilateral are used to extrapolate backwards, forming a new quadrilateral that represents the location of the inflowing air three hours earlier, assuming a constant wind speed and direction over the three-hour period.

The 850-hPa level was chosen because this level has been shown to be representative of the low-level moist inflow into a storm (Harnack et al., 1999). This technique was used for all parameters, with two exceptions. Recognizing that the inflow to the area of the event is significant at lower levels, the 850-hPa winds and the storm motion were sampled upstream of the quadrilateral box's location at each time period. Thus, to represent the 850-hPa winds and storm motion at time t0, the winds at the backtracked location for time t-3 were used, and so on for the remaining two time periods.

Those variables that represent the ambient synoptic conditions were not subject to this backtracking procedure. Instead, the calculations for these synoptic variables at

all three time periods were made in relation to the actual site of the flash flood. Table 4 notes whether a variable was characterized as local (L) or synoptic (S).

Table 4. Variables included in the discriminant analysis

Variable	***Source***	***Abbreviation***	***L/S***
Day	Storm Data/Hourly Precipitation Data	Day	L
Hour	Storm Data/Hourly Precipitation Data	Hr	L
Winds: 850, 700, 500, 300, 200 hPa	NARR	S850, D850, etc.	L
Storm Motion	Derived from NARR	MBESpd, MBEDir	L
1000-700 hPa wind shear	Derived from NARR	MidShearSpd, MidShearDir	L
700-500 hPa wind shear	Derived from NARR	LowShearSpd, LowShearDir	L
850 hPa temperature	NARR	T850	L
850 hPa geopotential height	NARR	Ht850	L
1000-500 hPa thickness	Derived from NARR	Thck	L
Sea level pressure	NARR	SLP	L
Relative humidity: surface, 850, 700, 500 hPa	Derived from NARR	RH850, RH700, RH500	L
1000-500 hPa mean relative humidity	Derived from NARR	MeanRH	L
Dewpoint: surface, 850, 700 hPa	NARR	Tdsfc, Td850, Td700	L
Surface potential temperature	NARR	PotTsfc	L
Convective Available Potential Energy	NARR	CAPE	L
Convective Inhibition	NARR	CIN	L
1000-500 hPa Lifted Index	NARR	LI1000500	L
K index	Derived from NARR	Kind	L
Warm Cloud Depth	Derived from NARR	WCD	L
Vertical Velocity: 1000, 850, 700 hPa	NARR	VV1000, VV850, VV700	L
Precipitable Water (% normal)	NARR, BGM climate normal Precipitable Water	Pwat%	L
Surface runoff	NARR	Runoff	L

Table 4. (Continued)

Variable	***Source***	***Abbreviation***	***L/S***
Latitude/longitude	Storm Data/center of included counties	Lat/Lon	L
Divergence: 850 and 200 hPa	Derived from NARR	Maxlldiv, Minlldiv, Maxuldiv, Minuldiv	L
Distance to θ_e axis	Derived from NARR	ThetaeAxisD	S
R^2 of θ_e axis	Derived from NARR	ThetaERsq	S
Thickness diffluence	Derived from NARR	ThickDiffWF	S
Soil Moisture	NARR	SoilM	L
Moisture Availability	NARR	MoistAv	L
Weekly antecedent precipitation	NRCC daily precipitation data	WeekAnt	L
Monthly antecedent precipitation	NRCC daily precipitation data	MonthAnt	L

Antecedent precipitation for periods of one week (7 days) and one month (30 days) was also included as a predictor. Antecedent precipitation comes from the NRCC's cooperative station precipitation database. For each event, the station in a flood or non-flood reporting county with the largest storm total precipitation amount was used as the location of the antecedent totals. In the case of a tie, the station reporting the higher weekly total was chosen.

For the synoptic variables, the field within the entire domain of the grid was calculated, and values or gradients at specific points were selected to represent the large-scale field. The ridge axis of θ_e at 850 hPa was determined by finding the maximum θ_e for each latitudinal row of data points, and then fitting a regression line to these points with longitude as the predictor (see Figure 4 for examples).

Since the NARR grid is not aligned with latitude and longitude, but, rather, each row slopes from northwest to southeast, new rows were defined to correct for the potential bias of the eastern end of the row being approximately four and a half

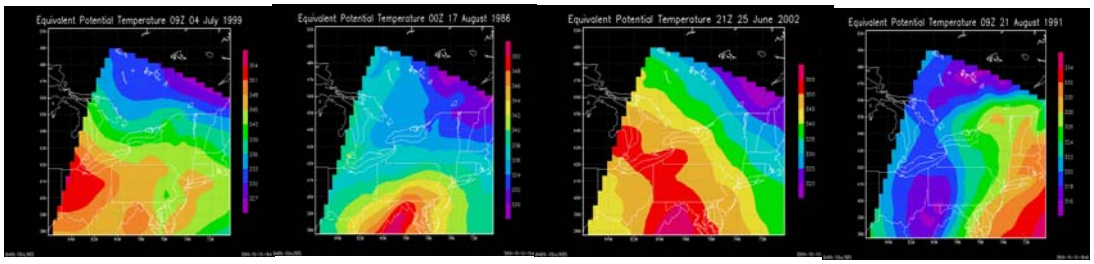

Figure 4. θ_e maps to illustrate examples of θ_e ridges
(parameter values, from left to right: 0.26, 0.5, 0.75, 0.98)

degrees latitude south of the western end of the row. The process for defining these new rows of approximately equal latitude is illustrated in Figure 5. This new method results in rows that slope by roughly one degree of latitude from west to east, and the results indicated significantly less biasing due to the latitude differential than the NARR rows did. The strength of the θ_e ridge was determined by the strength of the correlation (R^2) of the longitude with the maximum θ_e values for each row. The averaged values of θ_e for the quadrilateral flood area were also determined to represent the environmental θ_e values during the flash flood events. Finally, the distance from the axis of the regression-based θ_e ridge to the midpoint of the flood quadrilateral area at the latitude of the flood (representing the location of the flood) was recorded as a measure of the distance between the ridge axis and the flood.

Because the NARR grid is not aligned with latitude and longitude, but, rather, each row slopes from northwest to southeast, new rows were defined to correct for the potential bias of the eastern end of the row being approximately four and a half degrees latitude south of the western end of the row. The process for defining these new rows of approximately equal latitude is illustrated in Figure 5. This new method results in rows that slope by roughly one degree of latitude from west to east, and the results indicated significantly less biasing due to the latitude differential than the NARR rows did. The strength of the θ_e ridge was determined by the strength of the

correlation (R^2) of the longitude with the maximum θ_e values for each row. The averaged values of θ_e for the quadrilateral flood area were also determined to represent the environmental θ_e values during the flash flood events. Finally, the distance from the axis of the regression-based θ_e ridge to the midpoint of the flood quadrilateral area at the latitude of the flood (representing the location of the flood) was recorded as a measure of the distance between the ridge axis and the flood.

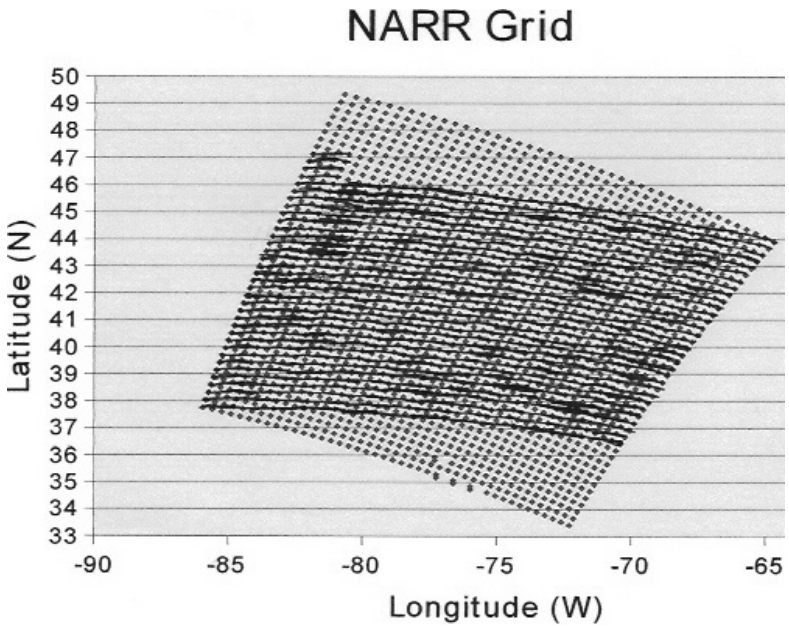

Figure 5. Illustration of modified rows used in θ_e ridge calculations

Thickness diffluence has been previously noted as a potential indicator of heavy precipitation and flash flooding because it indicates the presence of low-level convergence, upper-level divergence, or both (Funk, 1991). Thickness diffluence was determined by calculating north-south thickness gradients. Gradients were calculated over a 320-km (10 grid point) north-south distance at two longitudes: 10 grid points west of the flood location and at the longitude of the flood location. The midpoint of the area reporting flash flooding was designated as the reference point for these spatial calculations. A single variable to represent the thickness diffluence was derived by

determining the ratio of the thickness gradient north of the flood's latitude to the thickness gradient south of the flood's latitude. The north/south ratio for the grid points located at the longitude of the flood was then subtracted from the north/south ratio located west of the flood. A negative value for this parameter would indicate thickness diffluence, and a positive ratio would indicate thickness confluence. See Figure 6 for examples of this parameter.

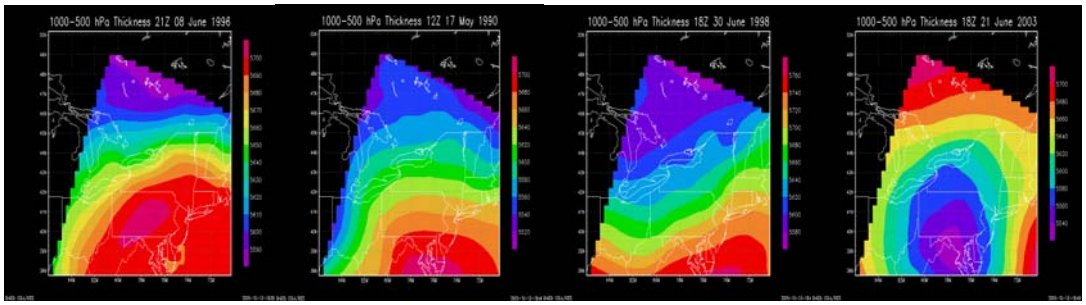

Figure 6. Thickness maps to illustrate examples of the thickness diffluence parameter (parameter values, from left to right: -15.12, -1.56, 0.01, 5.98)

The final parameter of the dataset is the divergence at lower (850 hPa) and higher (200 hPa) levels. The 850-hPa level represents the low-level inflow to the storm; the 200-hPa level approximates the jet stream. First, a Cartesian coordinate system locally defined by the grid was determined for each grid point, and grid-relative winds for each point were derived from the NARR's Earth-relative winds (u and v) using the following system of equations:

$$u' = u \cos \alpha - v \sin \alpha$$

$$v' = u \sin \alpha + v \cos \alpha$$

Here, α is the angle between the Earth-relative (latitude-longitude) and grid-relative coordinate systems. The convergence and divergence (div) were then calculated by finding the centered difference for each grid point. This is described in the equations below:

$$div = du/dx + dv/dy$$

$$du/dx = u'(x+1) - u'(x-1)/\Delta x$$

$$dv/dy = v'(y+1) - v'(y-1)/\Delta y$$

where x and y are the distances between the points defined by the local Cartesian coordinate system. Once the fields of lower-level and upper-level divergence had been found, these values were represented by the maximum and minimum values within the quadrilateral area containing the event, as well as the average divergence within this area.

Discriminant analyses were used to assess the parameters described above. The goal of these analyses was to determine which parameters were best able to differentiate between the flash floods and each non-event dataset at each time period, as determined by the Kuiper skill score (KSS) (Wilks, 1995). This approach is similar to that used in Hirsch et al. (2002). For each pairing of a non-flood dataset with the flash floods (flood/heavy, flood/watch, and flood/random), separate discriminant analyses were run for all cases and for those cases identified as convective in nature by the subjective and the objective classification schemes. Cross validation was used to check the validity of the discriminant classification with regard to independent data.

In the cross validation, a discriminant model was calculated for the *k* members of the dataset by removing one member of the dataset for each of *k* iterations. The value of the data point that is removed is predicted by the remaining members of the data set, and the error of the prediction is used in calculating a KSS for the cross validation. In this approach, separate trials of the cross validation were run, with each

trial holding one of the variables exhibiting the largest KSS from the discriminant analysis constant. Both the discriminant analysis and the cross validation were run for one variable, as well as for combinations of two and three variables. In general, combinations of up to three variables generated an improvement in the KSS of the discriminant analysis and the cross validation, and avoided over-fitting of the data (see Figure 7).

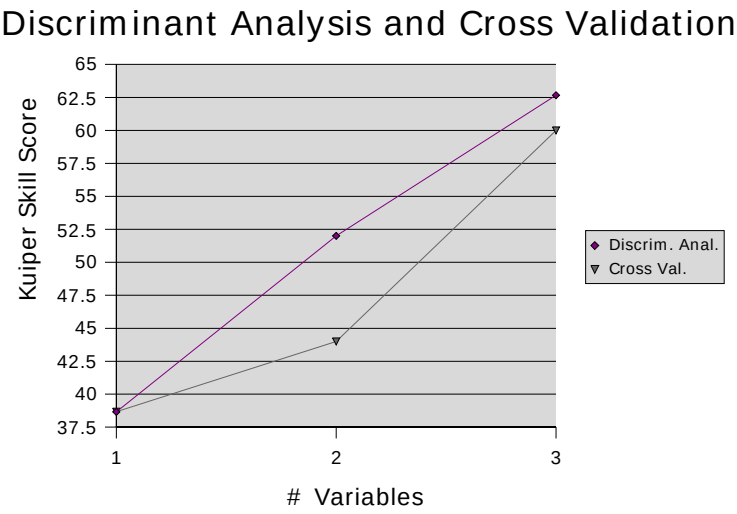

Figure 7. Example of Discriminant Analysis and Cross Validation (Flood/heavy, t0). The best combinations of 1 and 3 variables are reliable; the best two-variable combination is not.

CHAPTER THREE

RESULTS

Flash Flood Climatology - Temporal Variability

The vast majority of flash floods occurred in the late afternoon and through the evening (Figure 8). These late afternoon and evening events are dominated by spring and summer (warm-season) events. A secondary maximum occurs in the morning hours. These events tend to occur more often in the fall, winter, and early spring (cold-season events).

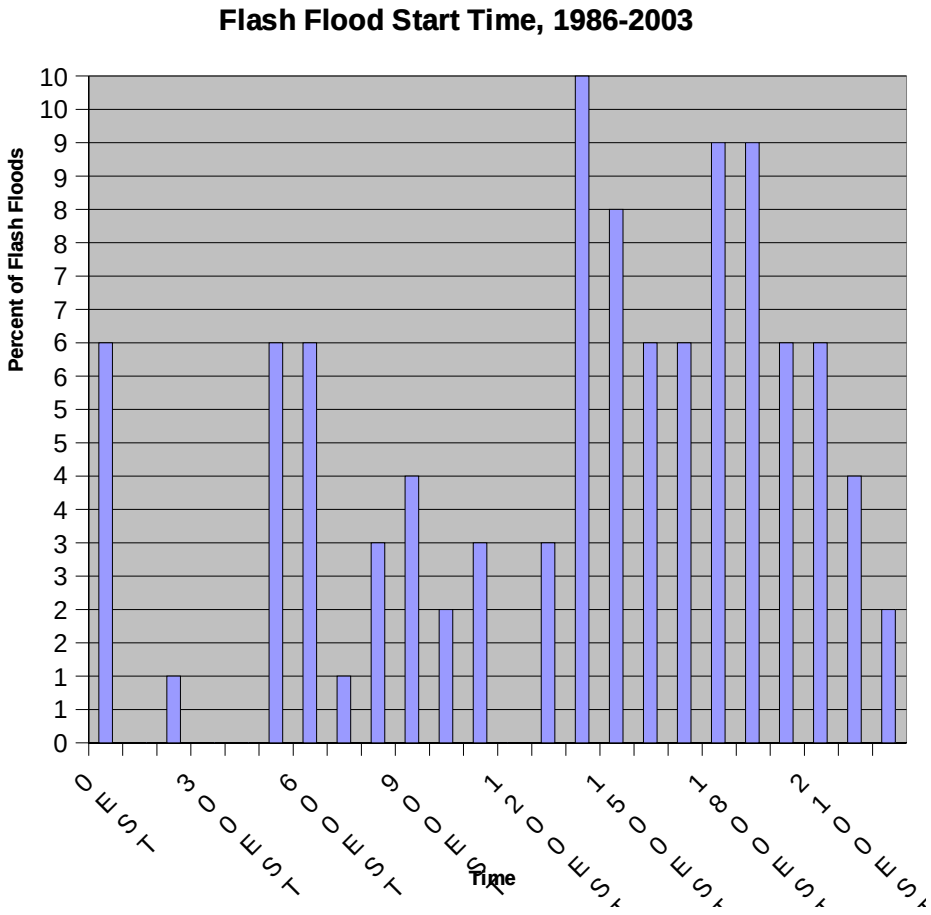

Figure 8. Diurnal distribution of flash floods

The annual peak for flash floods comes in the summer (Figure 9). Flash flood activity increases through the spring months, peaking in June. Flash floods continue to be common through July and August, before waning in the fall.

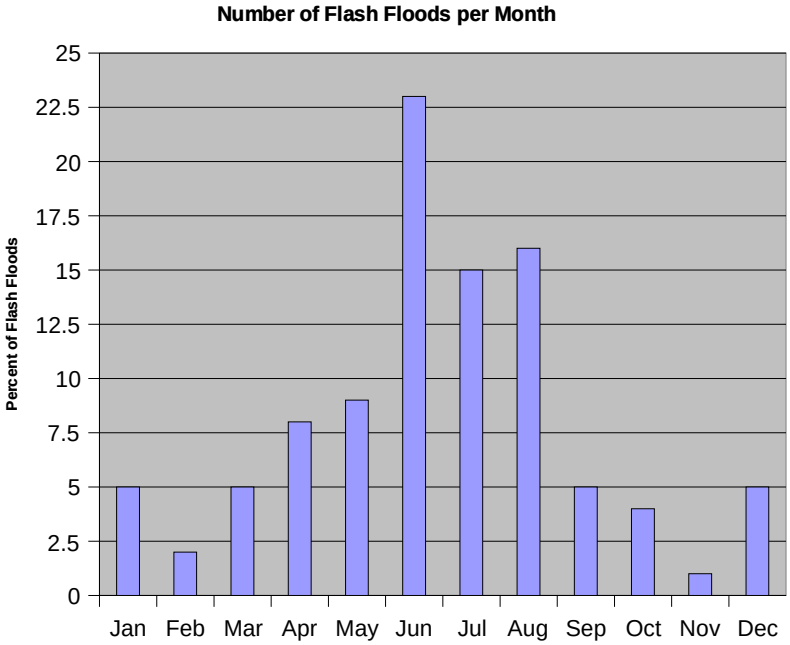

Figure 9. Annual distribution of flash floods

Flash flood climatology -Spatial variability

Flash floods tend to occur most often in the Southern Tier of New York State, Bradford County in Pennsylvania, and to a lesser extent along the easternmost counties of the CWA in New York State (Figure 10). The secondary maximum along the eastern edge of the CWA appears to be a function of the large area of these counties – they tend towards the average in terms of flash floods per county area (Figure 11). However, the counties in the New York Southern Tier, as well as Bradford County in Pennsylvania, remain the focus of flash flood activity in the CWA when taking each county's area into account. This peak area of flash flood activity is magnified when considering the relatively small area of Chemung, Tioga, and

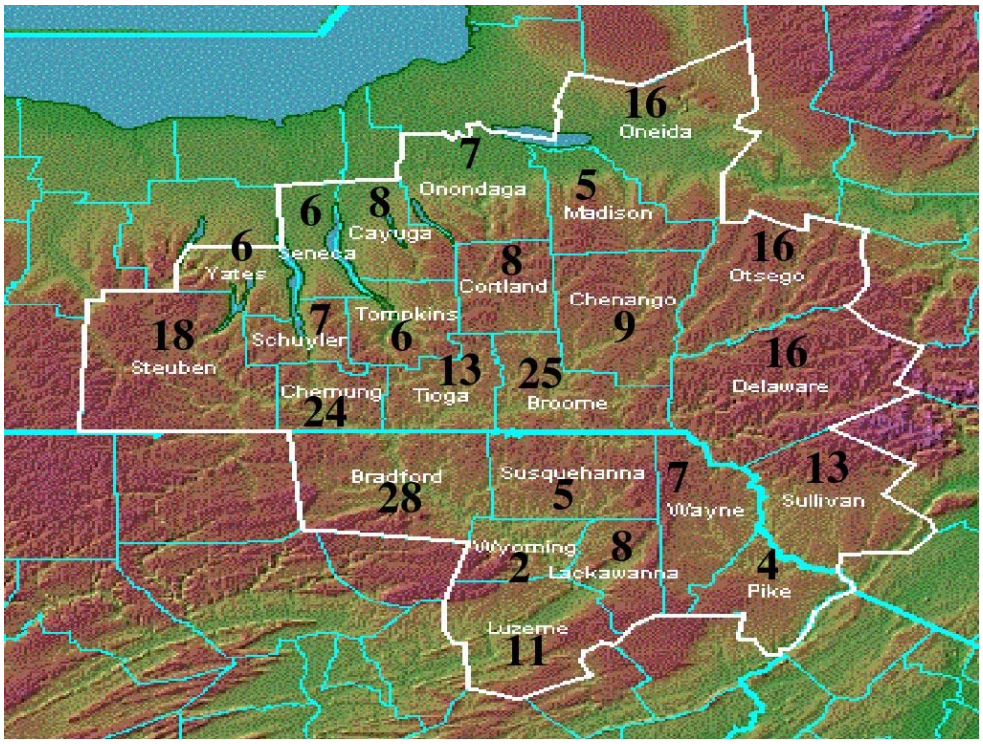

Figure 10. Spatial distribution of flash floods

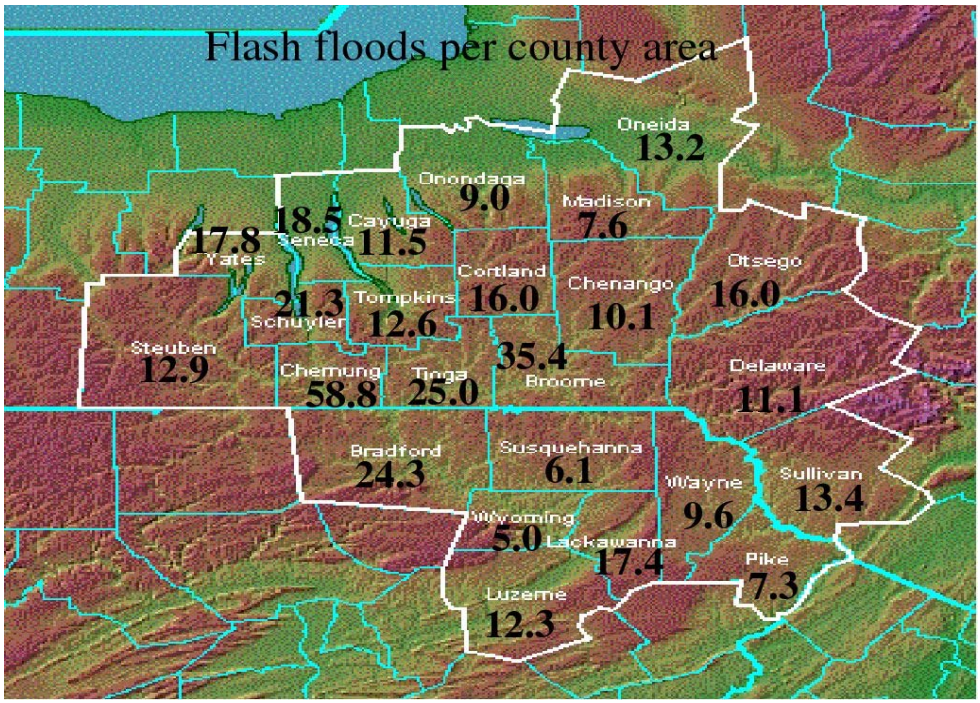

Figure 11. Spatial distribution of flash floods normalized by county area

Schuyler counties. A possible non-meteorological effect on the spatial distribution of the flash floods is the location of the National Weather Service office in Binghamton (Broome County), which may lead to a reporting bias from the surrounding counties. Additionally, two small counties to the north, Yates and Seneca, become more prominent as their area is taken under consideration. The high frequency of flash floods in Lackawanna and Luzerne counties stands out in comparison to the surrounding counties. This is likely due to the topography and land use of the area, with two large urbanized areas (Scranton and Wilkes-Barre) occupying a long, narrow valley.

Climatology of Flash-Flood-Producing Rainfall

The sparse nature of the rain gauge network, as well as the convective nature of most flash flood-producing storms, limits the accuracy of rain gauge measurements as a measure of the precipitation contributing to a given flash flood. The maximum reported 48-hour rain gauge totals are greatest in the summer and fall, with the all of the fall events exceeding 3.8 cm (1.5 inches) (see Figures 12-15). In contrast, many of the smaller amounts were recorded in the spring and summer months. This suggests that fall events tend to occur from relatively long-duration events that cover a large area, where as spring and summer events are more often comprised of short-duration, spatially limited convective events. During winter events, snowmelt significantly contributes to the runoff; therefore, rain gauge reports tend to be less than in the other seasons. In both spring and summer, rain gauges report large numbers of high and low precipitation events. This may result from the mesoscale nature of flash-flood producing events during this time of year. In other words, the wide range of warm-season rain gauge reports may occur because some of these events "hit" a rain gauge, while others "miss". A second explanation may be that high antecedent soil moisture during this time of year – particularly in spring, when snow has recently melted - has

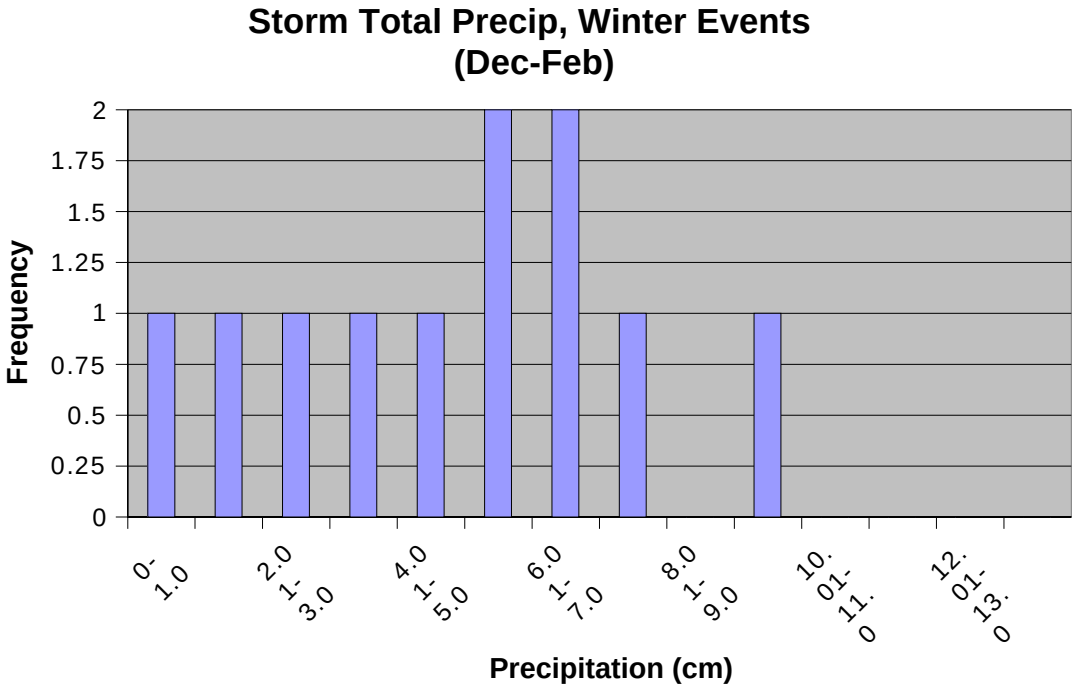

Figure 12. Maximum reported flash flood 48-hour rainfall, winter

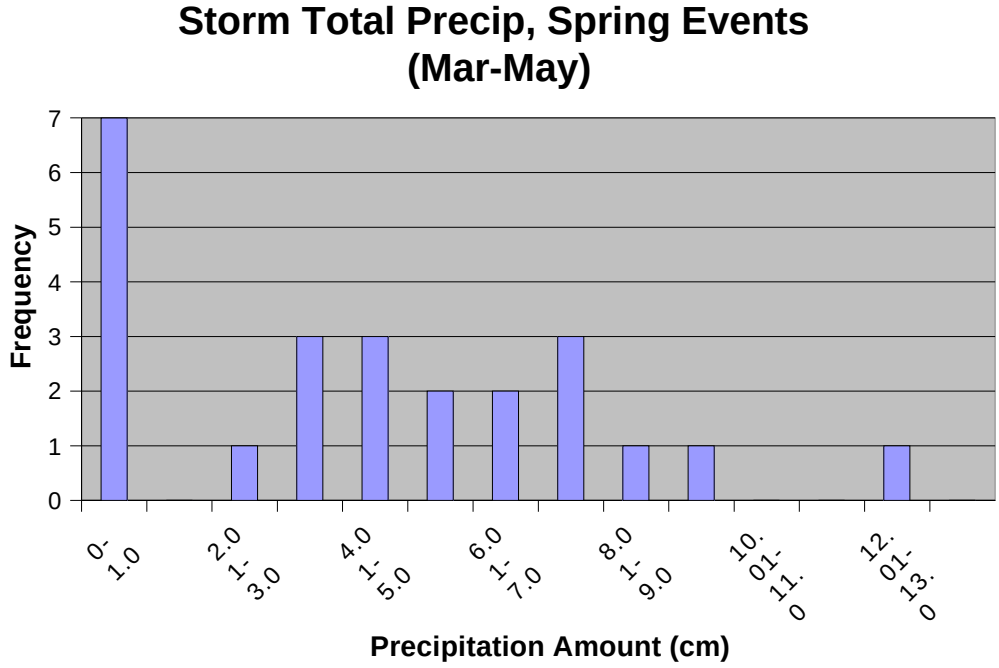

Figure 13. Maximum reported flash flood 48-hour rainfall, spring

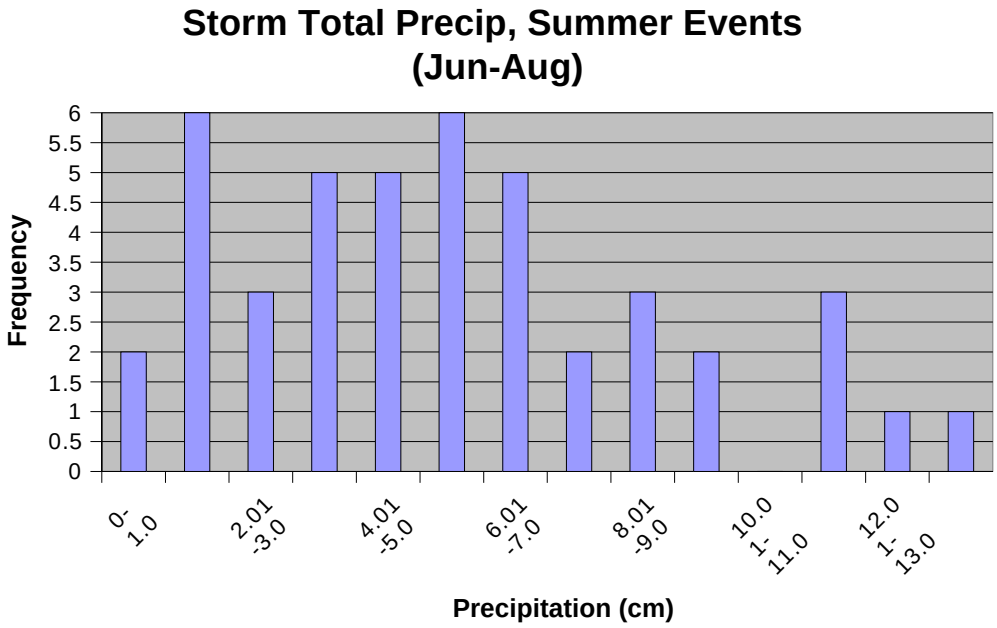

Figure 14. Maximum reported flash flood 48-hour rainfall, summer

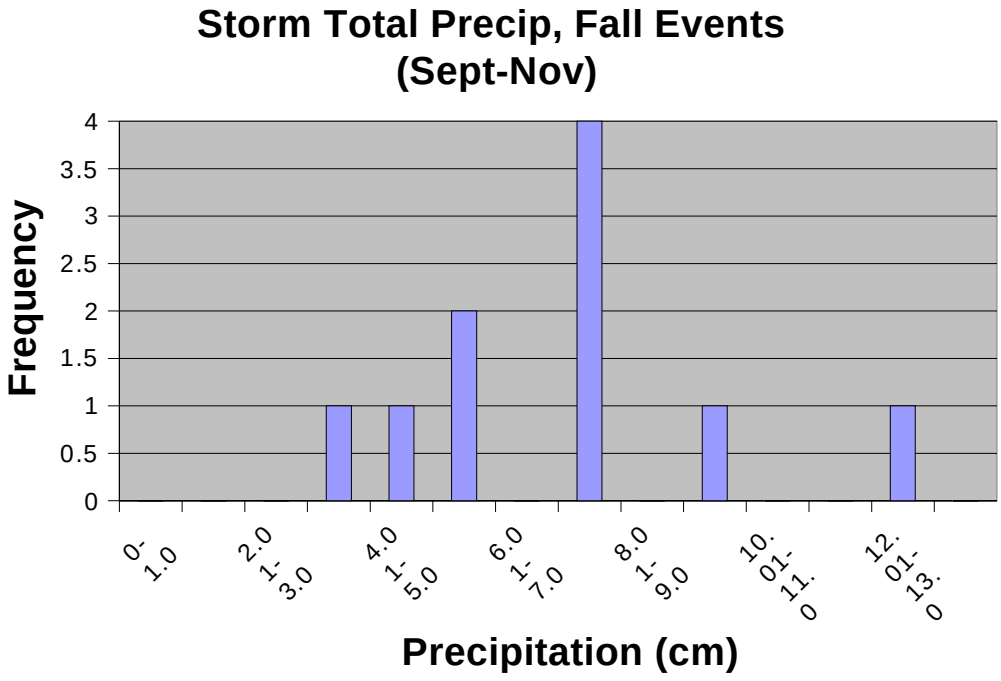

Figure 15. Maximum reported flash flood 48-hour rainfall, fall

left conditions ripe for flooding, susceptible to even a small amount of precipitation. There may be a seasonal dependence to the synoptic pattern producing these values of antecedent soil moisture, such that it occurs more regularly in the spring and summer months than in the fall.

Antecedent Precipitation Climatology

In general, flash flood events tended to occur during periods of above-normal precipitation. The annual median climatological 7-day precipitation total as determined by the procedure outlined in the "Data and Methodology" section is 1 cm (0.4 inches). The median for all counties reporting a flash flood for the 7-day period preceding the flood is 5.75 cm (2.26 inches). For the 30-day period preceding a flash flood, the median is 11.8 cm (4.64 inches). In contrast, the climatological median for a 30-day period is 5.66cm (2.23 inches).

It should be noted that this value is approximately 2 cm to 2.5 cm (0.78" to 0.98") lower than the normal monthly precipitation for stations located in the BGM CWA. This deficit is likely due to the exclusion of all flash flood years from the climatology. The occurrence of multiple flash floods within the same 7- or 30-day period, contributed to this difference as well. The difference between the cumulative distributions of antecedent precipitation for the climatology and the flash flood cases, as determined by a chi-squared test, is statistically significant for $P < 1\%$ (Figures 16, 17).

Properties of Flash Floods

The following sections will describe the environmental characteristics of the flash floods and compare them with the random events. These results are based on the NARR, and, as such, are at the spatial resolution of the NARR. All results are for time t0, unless otherwise indicated.

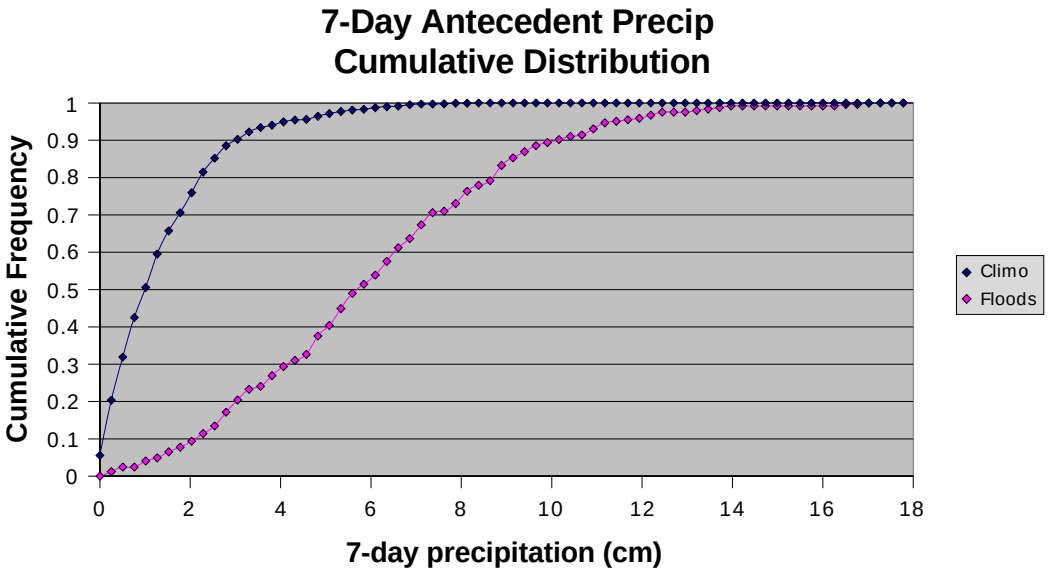

Figure 16. Weekly antecedent precipitation cumulative distributions, flash floods and climatology

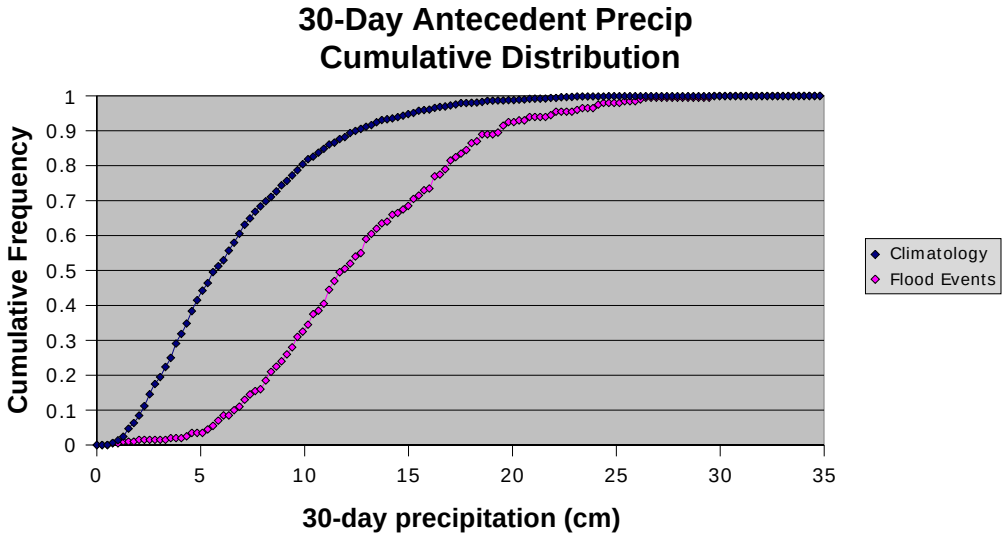

Figure 17. Monthly antecedent precipitation cumulative distributions, flash floods and climatology

Wind Fields

The majority of flash flood cases included 850 hPa wind directions ranging from southerly to westerly or slightly west-northwesterly (180 to 280 degrees) (Figure 18). This generally agrees with the finding of Harnack et al. (2001) that low-level southerly winds are often found in proximity to heavy rainfall events. Roughly 25% of the cases had 850 hPa winds with an easterly component (60 to 130 degrees). These cases had no preferred seasonality or antecedent precipitation, but they did fall into two categories. Most of these cases had a combination of high low-level relative humidity, relatively low CAPE (< 115 J/kg), and a lifted index greater than or approximately 0 degrees C. They were typically accompanied by backing winds in the 1000 to 700 hPa layer. Many of the cases with southeasterly winds were located in northeastern Pennsylvania or southern New York, which suggests that topography may have played a role in the forcing of these events.

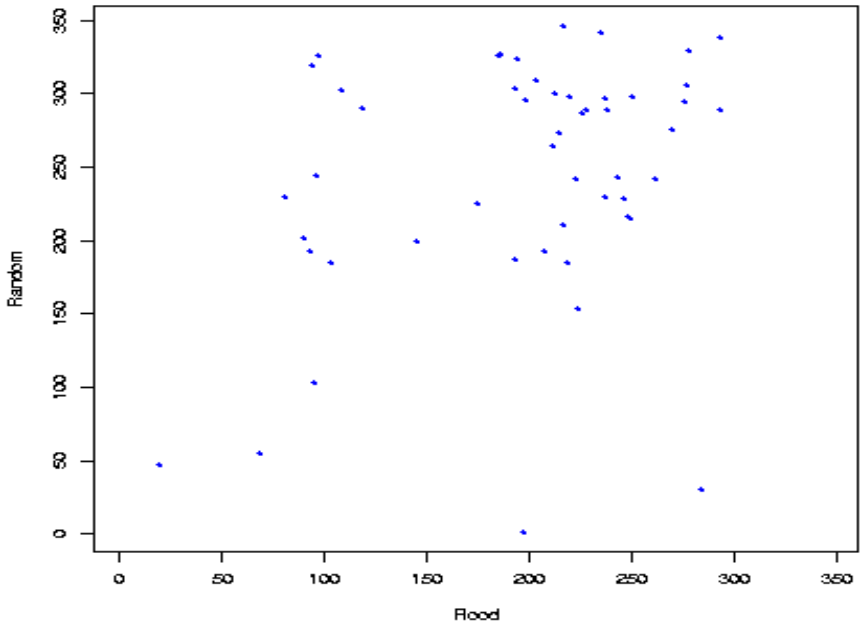

Figure 18. 850-hPa wind direction (degrees)
(ordinate: random events; abscissa: flood events)

Only two cases had northwesterly 850 hPa winds greater than 290 degrees. This is a pronounced contrast to the random cases, where 47% of the events were associated with northwesterly winds of approximately 290 degrees or greater. These cases were convective events, with relatively low RH, particularly at low levels, along with moderate to high CAPE and low precipitable water. They were preceded by antecedent precipitation and soil moisture that exceeded the flash flood average.

Finally, one exception stood out in that its 850-hPa wind direction was northerly (19.5 degrees). This case was caused by thunderstorms along a back-door cold front and exhibited relative humidities near or below the flood average for all levels, a fairly high CAPE (620 J/kg), and antecedent soil moisture near the flood average.

The mean 850-hPa wind speed was 8.42 m/s, with an upper quartile of about 11 m/s and a maximum of 22 m/s (Figure 19). These values are similar to those of the random events. The three cases with a speed >17 m/s all had a relative humidity greater than 80% between the surface and 700 hPa. These cases also had CAPE <250 J/kg. Precipitable water values for all three cases were greater than the mean

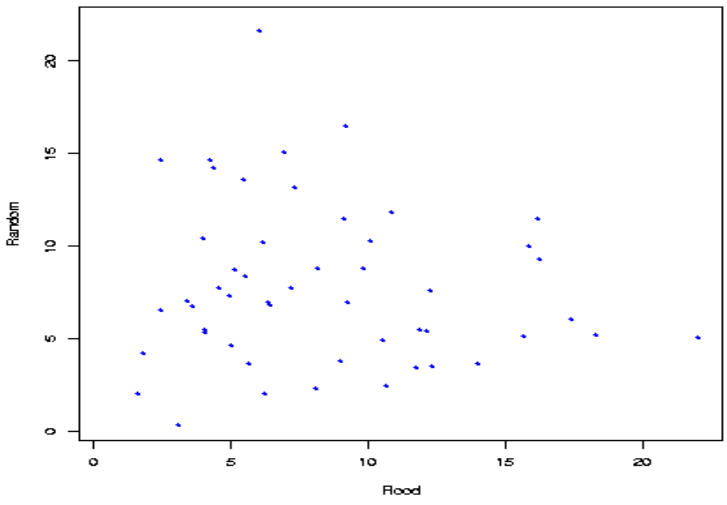

Figure 19. 850-hPa wind speed (m/s)

precipitable water as a percent of normal for all flash floods. Finally, two of the cases had especially high weekly (>12 cm or 4.75") and monthly (>19.7 cm or 7.75") antecedent precipitation totals.

Much like at 850 hPa, winds at 700 and 500 hPa were mostly southerly to westerly. The few cases with a large easterly component tended to have moist antecedent soil conditions, low measures of absolute moisture (such as precipitable water and dewpoint), but high relative humidity. These cases were mostly located in the southeastern portion of the CWA. Several cases had northwesterly mid-level winds, most of which occurred in the eastern portion of the CWA. These cases were commonly moderate to high CAPE events with low to moderate precipitable water, and relative humidity, but high dewpoints, and weak upper-level winds.

Lower-level winds (from 1000 hPa to 700 hPa) often featured large shifts in direction: more than 70% of the cases had low-level directional shear larger than 50 degrees (Figure 20). The flood events often had much larger lower-level shear than the random events. Veering and backing with height in this layer were equally common, although backing tended to be larger in magnitude. Those cases with

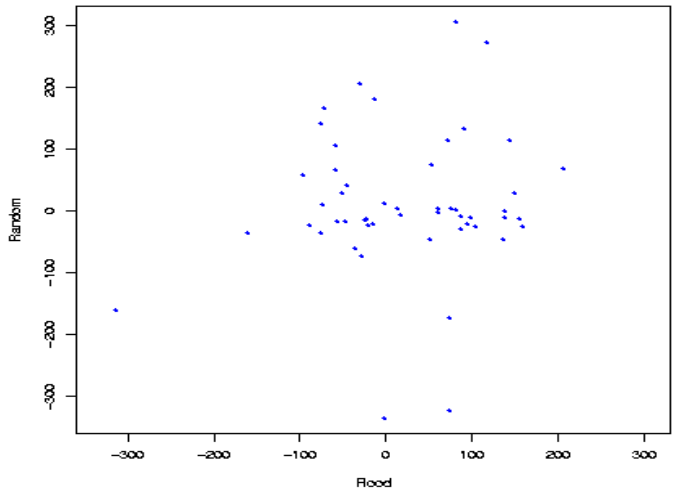

Figure 20. Low-level directional shear (degrees)

veering lower-level winds tended to be located in the more northern areas of the CWA. They also had lower relative humidities and often had a southerly to westerly 850 hPa wind direction. In contrast, those cases with backing more often affected the southern portion of the CWA, with higher relative humidities. Lower level speed shear was often less than 10 m/s (Figure 21), which is quite similar to the values of the random events. Those floods exceeding this threshold were often in the northern half of the CWA, and most of them came in the morning or afternoon of the cooler months: May, September, and October. Events with large lower-level speed shear typically also had large directional sheer for this layer. However, these cases were often associated with weak speed and directional shear above this layer.

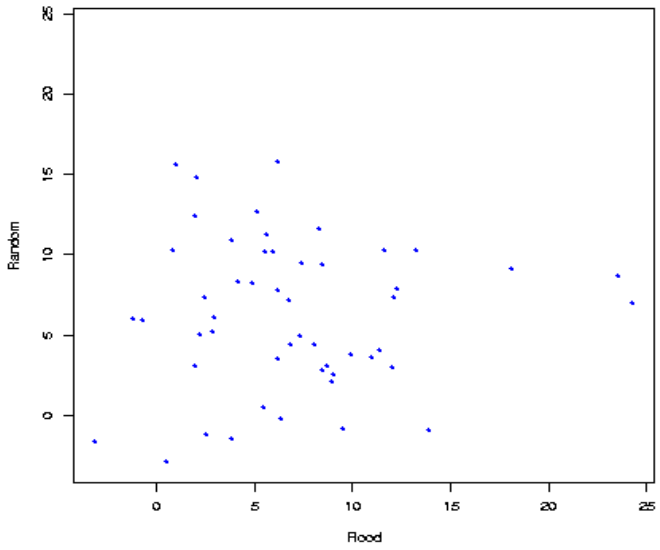

Figure 21. Low-level speed shear (m/s)

Directional shear and speed shear at mid-levels (between 700 hPa and 500 hPa) were often weak (Figures 22 and 23). The majority of the flood events had similar shear values to the random events, but several flood cases had much larger shear than any of the randoms. More than half of the events had directional shear of

less than 10 degrees. However, several cases featured either veering or backing with height of 50 degrees or greater. The majority of cases with large veering had 850-hPa wind speeds and storm motions larger than the flash flood mean. Most of the cases with large backing had winds with an easterly component at 850-hPa. Weak speed shear was the norm, as most cases had a speed shear less than 10 m/s. Of the six exceptions that exceeded this amount, most had large relative humidity at the surface (>89), were above of the mean flash flood weekly antecedent precipitation, and surpassed the mean monthly antecedent precipitation.

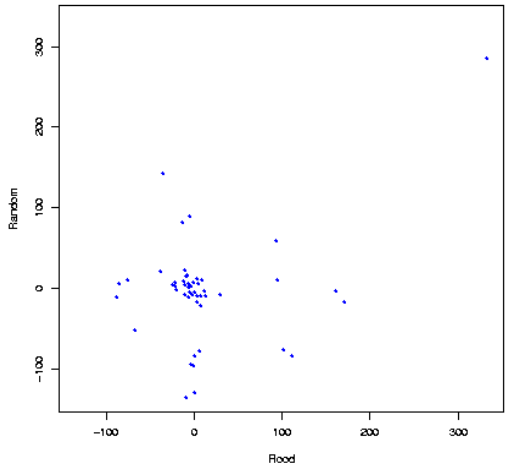

Figure 22. Mid-level directional shear (degrees)

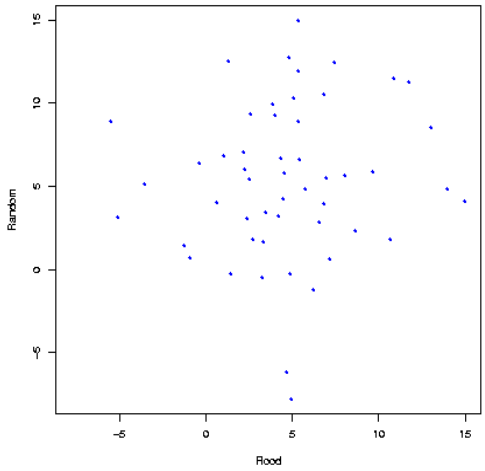

Figure 23. Mid-level speed shear (m/s)

Storm motion vectors generally varied from southeasterly to westerly, except for one case with northeasterly motion, three cases with east-southeasterly storm motion, and two cases with storm motion from the northwest (Figure 24). This is in contrast to the westerly to northwesterly preference of the random cases. Those cases with atypical storm motion directions did not necessarily share the same wind direction at 850-hPa, but they did tend to be on either the easterly or northwesterly

side of the mean direction, respectively. The case with northeasterly motion had very high relative humidity from 100 to 850 hPa, but was drier aloft. Dewpoints for this case were relatively low, however, so it was a cooler event with a precipitable water amount near the flash flood mean. The east-southeasterly cases had relatively high moisture at the surface and 850 hPa, and one of the three cases maintained this high moisture up to 500 hPa, while the other two were relatively dry in the mid-troposphere. Despite high relative humidity for at least a portion of the lower troposphere, the dewpoints were low, resulting in precipitable water values that are not significantly larger than normal compared to most flash floods (up to 174% of normal). The two cases with northwesterly storm motion had temperatures and dewpoints above the flash flood mean, combined with moderate CAPE and high antecedent precipitation.

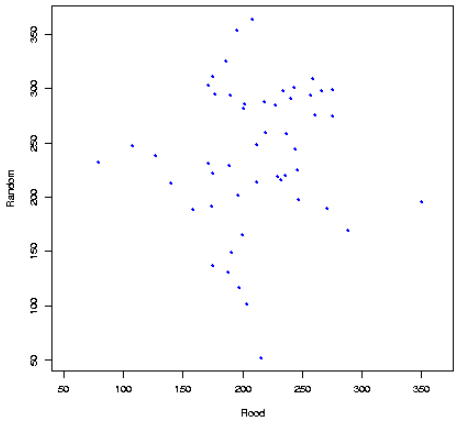

Figure 24. Storm motion direction (degrees)

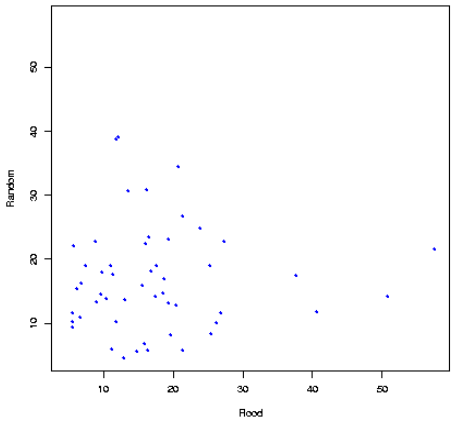

Figure 25. Storm motion speed (m/s)

Storm motion speeds of the flood cases are similar to the random cases in that they are usually not very fast, with a mean of 16.35 m/s and 75% of the cases less than 20 m/s (Figure 25). Most storm motion speeds are similar to the wind speed at 850-hPa, but there are cases of high storm motion speeds with weak 850-hPa winds and

vice versa. The cases with the fastest storm motion were typically associated with high weekly antecedent precipitation and antecedent soil moisture. However, the converse was not necessarily true – many of the cases with slow storm motion also had relatively high antecedent precipitation in comparison to the other flash floods. The faster-moving cases contained moderate to low CAPE, and differed in their atmospheric moisture content, suggesting that they represented both convective and non-convective scenarios. The case with the fastest storm motion was an outlier in several other parameters as well. It had the fastest 850-hPa wind speed (45 m/s), a very moist lower troposphere with a precipitable water of 289% of normal, fast upper level winds (>50 m/s at 300 and 200 hPa), and high antecedent precipitation and soil moisture.

Upper level winds (300 and 200 hPa) were quite similar to those of the random events, with a primarily southerly to westerly direction, and a few exceptions either northwesterly or southeasterly (Figure 26). Much like the comparison between storm motion and 850-hPa, about half of these exceptions in the upper troposphere corresponded with similar wind direction and storm motion in the lower troposphere. Differences in upper tropospheric wind direction did not appear to be related to significant trends in any other parameters. Wind speeds at the upper levels were typically between 20 and 40 m/s, but reached as high as 65 m/s at 200 mb and as low as 3 m/s at 300 mb (Figure 27). The cases with fast upper level winds also had fast storm motion in most instances. These cases were also typically associated with lower surface pressure. For those cases in which upper level winds were anomalously slow, surface pressure and temperature tended to be higher, and weekly antecedent precipitation tended to be lower.

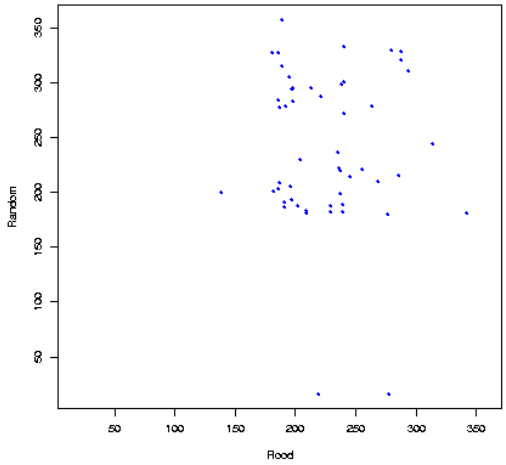

Figure 26. 200-hPa wind direction (degreees)

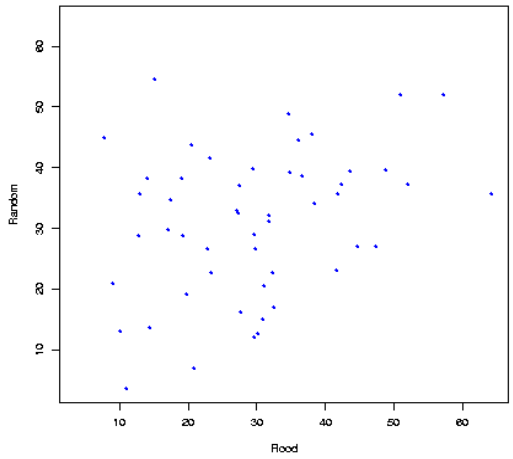

Figure 27. 200-hPa wind speed (m/s)

Atmospheric Moisture

Dewpoint temperatures proved to be a more consistent indicator of moisture than relative humidity. Dewpoints typically remained within a range of 10 Kelvins for a given pressure level, whereas relative humidity contained a spread of as much as 40%. These measures of atmospheric moisture also show distinct difference in spread between the flood and random cases, with the flood cases typically having more lower and middle tropospheric moisture. Dewpoints at 700 hPa were almost all between 269 and 280 K, with one anomalously low case of 259 K (Figure 28). This one case, which occurred in October, also had an 850-hPa temperature, 850-hPa height, 1000-500 hPa thickness, and K index significantly lower than all other flash floods. However, other parameters, such as relative humidity at all levels except 700 hPa, precipitable water, and weekly antecedent precipitation, were very near to their respective flash flood means. At 850 hPa, the dewpoints tended to be between 280 and 290 K. (Figure 29) Surface dewpoints were generally between approximately 285 and 295 K (Figure 30). In general, cases with higher dewpoints were associated

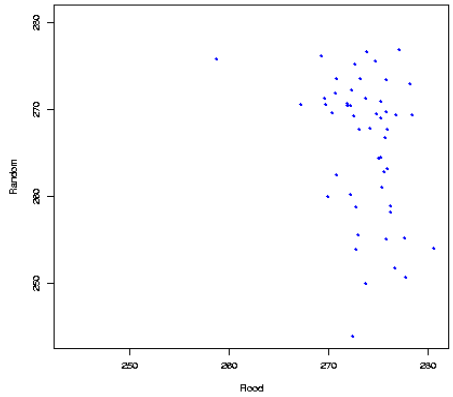

Figure 28. 700-hPa dewpoint temperature (Kelvins)

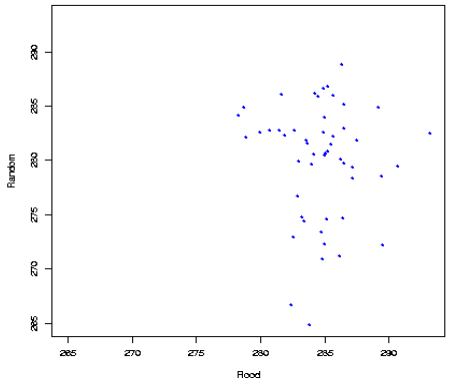

Figure 29. 850-hPa dewpoint temperature (Kelvins)

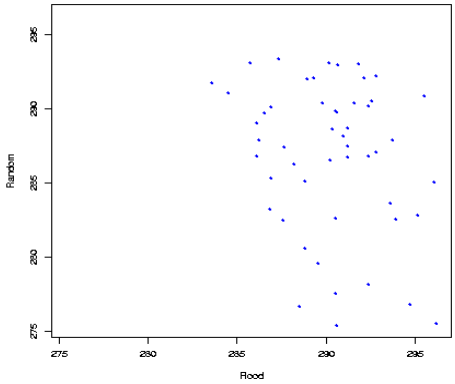

Figure 30. Surface dewpoint temperature (Kelvins)

with higher CAPE and, therefore, generally tended to be convective events. The converse also proved to be true, especially at the surface – cases with lower dewpoints tended to be associated with lower CAPE, and were more likely to be non-convective.

The mean precipitable water, by percentage of normal, was 164% (Figure 31). All cases exceeded 100% of normal, but one-third of them (17 of the 51 cases) were between 100% and 150% of normal. In contrast, only 7 cases were greater than 200% of normal. Most of these cases with extremely large precipitable water occurred in May, October, or November. As with the other measures of atmospheric moisture, the precipitable water of most flood cases exceeded that of most random cases.

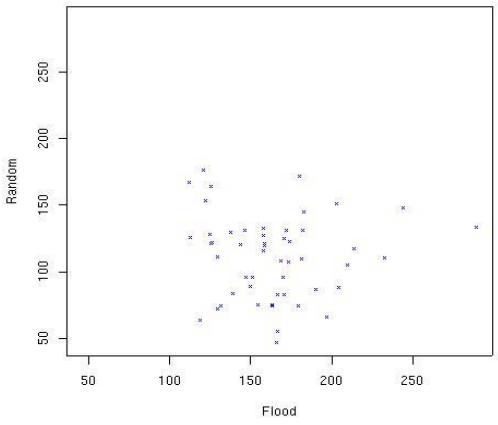

Figure 31. Precipitable water (% normal)

Thermodynamic and Convective Properties

Thicknesses between 1000 and 500 hPa ranged from 5560 to 5800 m (Figure 31). Higher thicknesses are associated with greater convective potential and more variable mean RH (Figure 32). Lower thicknesses typically accompanied the events occurring in spring and autumn: all but one event occurring in May and all events in September and October had thicknesses below the mean of all flash flood events. In general, the flood thicknesses tended to be larger than those of the random cases.

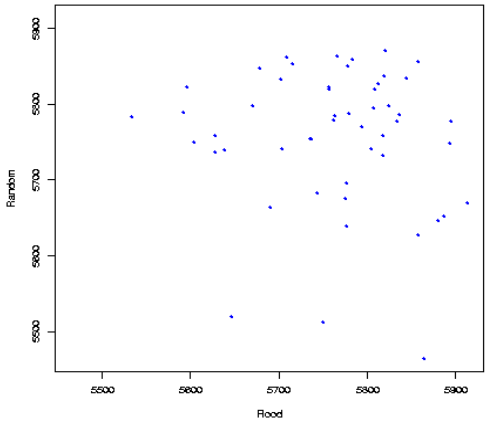

Figure 32. 1000-500 hPa thickness (m)

Bohl and Junker (1987) calculated a mean and standard deviation thickness for heavy precipitation by region for the eastern and central United States. In comparison to this standard for the northeastern U.S., one-third of the floods had thicknesses outside of one standard deviation of the mean thickness for the Northeast region, and several cases were within one standard deviation by 5 m or less. In general, it was slightly more common for cases to contain above-average thicknesses than below-average thicknesses. There was no seasonal signal in the departure from average thickness.

Measures of convective potential were, in most cases, moderate. CAPE rarely exceeded 1000 J/kg (six cases), with a maximum of 3286 J/kg (Figure 33). However, CAPE for the flood events was often much larger than for the random events. Many of the flood cases exceeded 250 J/kg, whereas very few random cases did. High-CAPE events tended to occur with higher temperatures and higher dewpoints. At the lower extreme, only two cases had zero CAPE. Low CAPE (i.e. non-convective) events occurred somewhat more frequently – 14 cases had a CAPE greater than 0 but less than 75 J/kg. There was no preference for a specific wind direction associated with high or low CAPE, and similarly, both atmospheric moisture and antecedent precipitation did not appear to be related to convective potential.

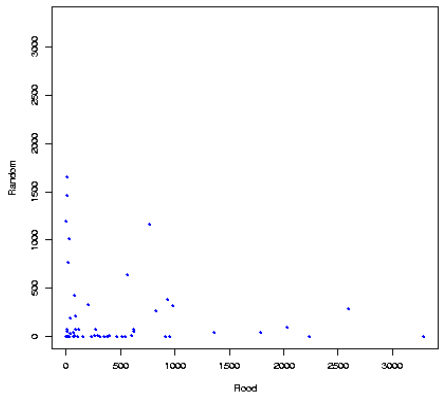

Figure 33. CAPE (J/kg)

Most cases had model-derived convective inhibition (CIN) between -10 and 0 J/kg (Figure 34). A negative value of CIN denotes convective inhibition; that is, the negative area in an atmospheric sounding that a parcel must overcome. Some had low CIN, down to a minimum of -40.5 J/kg. In contrast, only one case had positive CIN. Lifted index typically ranged from the upper-260's K to the mid-270's K, with a min of 263.5 and a max of approximately 285 K (Figure 35). K-index was generally in the middle 20's Celsius to lower 30's Celsius (not shown). Its distribution was skewed to the left with an outlying min of 10 degrees C. Neither CIN nor K-index appears to depend on winds, atmospheric moisture, or antecedent precipitation. Both the CIN and K-index differed from the flood to the random cases, with the floods typically having a larger CIN and the randoms having a larger K-index.

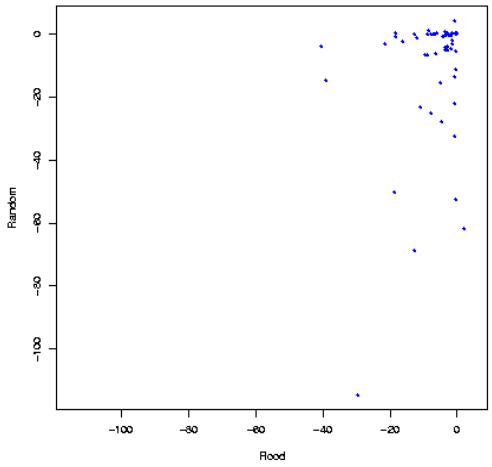

Figure 34. CIN (J/kg)

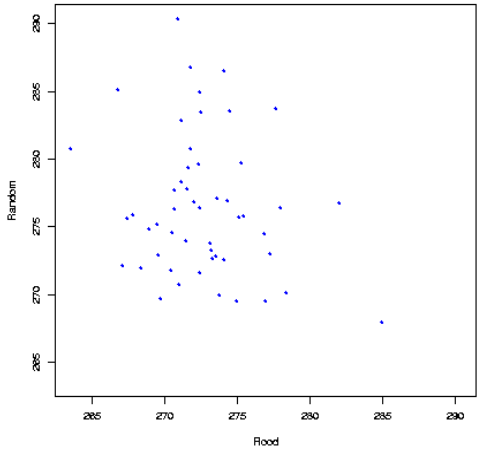

Figure 35. Lifted index (Kelvins)

Model-derived vertical velocities indicate that rising air associated with flash flooding is not necessarily present at the 32-km resolution of the NARR. Vertical velocities in the NARR are derived from horizontal divergence, which may lead to errors in their estimation. 17 of the 51 cases had NARR-derived vertical velocities greater than or equal to zero (implying sinking or vertically stationary air at 1000 hPa.

The 1000-mb level presents problems, however, because five cases had a sea level pressure less than 1000mb and several others may have had a station pressure less than 1000 hPa. At 850 hPa, 10 cases had positive vertical velocities in the NARR, about half of which corresponded with sinking air at 1000 hPa. At 700 hPa, 14 cases had positive vertical velocities. Many of these corresponded with positive vertical velocities at either 1000 hPa, 850 hPa, or both.

This result is counter-intuitive, but the spatial resolution of the data may offer an explanation. Because the vertical velocities were the average of at least four grid points over a minimum area of 1050 km^2, the interpretation of those cases with positive vertical velocities (i.e. sinking air) is that small-scale convection below the scale of the NARR appeared within larger-scale subsidence.

Antecedent Soil Moisture

Antecedent soil moisture appears to be one of the key components of a flash flood. Additionally, it appears to have a much larger magnitude for flash floods than typical climatological values, as suggested by the difference in the flood and random distributions of both rain gauge and model-derived antecedent precipitation and soil moisture. All cases had at least an inch of precipitation in the week leading up to the flood, with a range from one inch to six inches, with a mean of 8.1 cm (3.2 inches, Figure 36). In particular, October and November had the most consistently wet conditions, with all four events in these months receiving at least 7.6 cm (3") of rainfall in the week leading up to the event. The four cases with a weekly antecedent total of less than 3.8 cm (1.5") had a CAPE greater than 250 J/kg, but the next several highest antecedent totals were associated with cases of less than 100 J/kg CAPE. Wet antecedent conditions tend to persist for the longer term in advance of flash flood events as well. Monthly antecedent precipitation was no less than approximately 3.8

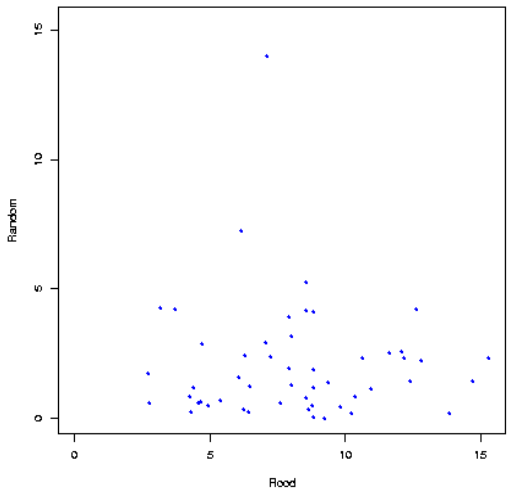

Figure 36. Weekly antecedent precipitation (cm)

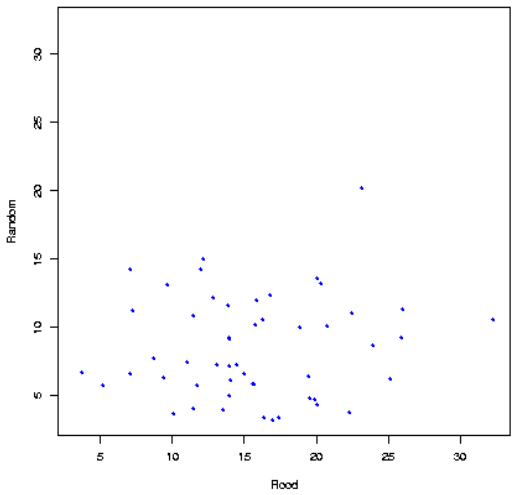

Figure 37. Monthly antecedent precipitation (cm)

cm (1.5") and reached as high as 32.3 cm (12.7"), straddling a mean of 15.6 cm (6.16", Figure 37). In general, the data suggest that flash flooding from both convective and non-convective events can occur regardless of whether antecedent precipitation is above or below the flash flood mean antecedent precipitation.

With high antecedent precipitation totals, soils are typically quite moist as a flash flood begins. NARR moisture availability in the uppermost 100 cm was as little as 18.65% and as high as 80.68%, averaging 58.38%. Only ten cases (roughly 1/5 of the flash floods) had moisture availability less than 50%. Similarly, soil moisture content in the uppermost 200 cm of the soil ranges from about 450 to 800 kg/m^2, with a mean of 638.1 kg/m^2. All but six cases have soil moisture greater than 550 kg/m^2 (Figure 38). Most cases with low NARR moisture availability and low NARR soil moisture had weekly antecedent precipitation near or above the flash flood mean. They usually occurred later in the warm season, from August through October, and they tended to be in the northern portions of the CWA. One likely explanation for this discrepancy is that the antecedent precipitation may have fallen early in the week and

permeated into the ground before the time of the flash flood. The other potential explanation is that the model parameterization of the soil moisture and moisture availability underestimated these values.

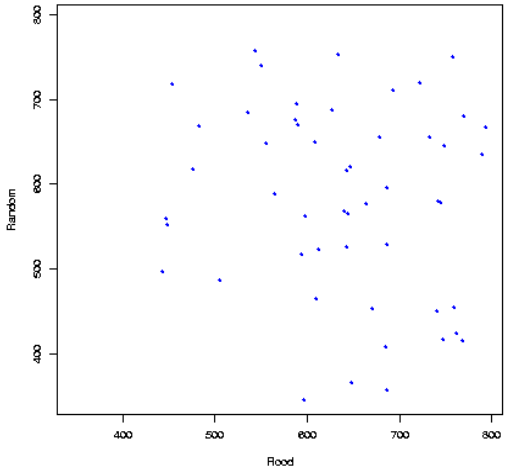

Figure 38. Soil moisture (kg/m^2)

Discriminant Analysis Results - F*lash Floods vs. Heavy Precipitation*

The parameters that best distinguished between heavy precipitation and flash flood events at the closest time to the event's occurrence were those indicating antecedent soil moisture, including weekly antecedent precipitation, soil moisture, and soil moisture availability (Table 5). Flood events tended to have larger observed and modeled antecedent soil moisture than heavy events. Model-derived soil moisture was the best single discriminator. Other significant individual discriminators included 850 hPa dewpoint (higher in heavy events than in floods) and the R^2 value representing the θ_e axis correlation (stronger correlation in heavy events, with the θ_e axis located farther east). The two-variable combination of warm cloud depth (larger for heavy events) and soil moisture improved the skill to 51.724 with a cross-validated skill of 44.828.

Table 5. Flood/heavy discriminant analysis results, all cases
(cross validated KSS in parenthesis)

Time	***One Variable***	***Two Variables***	***Three Variables***
t0	40.23 SoilM (37.931) 35.632 Td850 (35.632) 33.333 MoistAv (33.333) 33.333 WeekAnt (33.333) 28.736 ThetaERsq (28.736)	51.724 WCD, SoilM (44.828)	58.621 MBEDir, ThetaEAxisD, MoistAv (54.023) 58.621 D850, Maxlldiv, SoilM (47.126) 58.621 D850, CIN, SoilM (56.322) 58.621 D850, MBEDir, SoilM (54.023)
t-3	42.529 SoilM (42.529) 37.931 MoistAv (37.931) 33.333 WeekAnt (33.333) 31.034 ThickDiffWE (28.736) 31.034 ThetaEAxisD (31.034)	49.425 Avguldiv, MoistAv (47.126) 49.425 Minuldiv, SoilM (47.126) 49.425 Minuldiv, MoistAv (49.425) 49.425 LI1000500, MoistAv (44.828) 49.425 CAPE, SoilM (49.425) 49.425 MeanRH, MoistAv (47.126) 49.425 RH500, SoilM (47.126) 49.425 RH500, MoistAv (47.126) 49.425 RH700, SoilM (49.425) 49.425 Ht850, MoistAv (44.828) 49.425 S850, MoistAv (49.425)	63.218 S850, Minuldiv, MoistAv (60.92)
t-6	35.632 MoistAv (35.632) 33.333 WeekAnt (33.333) 33.333 T850 (33.333) 31.034 SoilM (31.034) 31.034 ThetaERsq (31.034)	47.126 ThetaERsq, WeekAnt (44.828) 47.126 Avguldiv, WeekAnt (42.529) 47.126 Td850, WeekAnt (42.529)	58.621 VV700, ThetaERsq, WeekAnt (49.425)

The best predictability resulted from combinations of three variables. They contained an indicator of antecedent soil moisture and wind direction. The combination of 850 hPa wind direction (more westerly for heavy events), CIN (slightly larger for heavy events), and soil moisture produced a skill score of 58.621. Nearly as skillful were the combinations of storm motion direction (more westerly for heavy events, similar to 850 hPa winds), distance to the θ_e axis, and soil moisture availability and 850 hPa wind direction, storm motion direction, and soil moisture.

Following the backtracking routine through the t-3 and t-6 times, both model-derived soil moisture at the t-3 and t-6 location and weekly antecedent precipitation at the site of the event remain the strongest distinguishing factors between these two types of events. At t-3, synoptic parameters - thickness diffluence (more common for heavy events), distance to the θ_e axis (further to the east with a stronger axis correlation for heavy events) - were important. At t-6, other significant parameters included the strength of the θ_e axis (R^2) and the 850-hPa air temperature (warmer for heavy events). A discriminant analysis including only those events classified as convective produced similar results.

Discriminant Analysis Results - Flash Floods vs. Non-verifying Flash Flood Watches

The parameter most able to differentiate between flash floods and false-alarm flash flood watches was the distance to the 850-hPa θ_e axis ridge (Table 6). The typical θ_e axis distance in the watch events had a larger magnitude than that of the flood events, regardless of whether the ridge was calculated to be west or east of the event. Other important variables included 850-hPa relative humidity (larger in watch events), wind direction at 850-hPa (more westerly in watch events, similar to the heavy events), and weekly antecedent precipitation (larger for floods). Notable combinations of variables from the flood/watch discriminant analyses included 850 hPa wind direction, weekly antecedent precipitation, and 700 hPa RH; and 850 hPa

wind direction, 850 hPa RH, and 1000 hPa vertical velocity. The watch events typically had larger mid- and upper- level relative humidities and slightly larger vertical velocities.

Table 6. Flood/watch discriminant analysis results, all cases (cross validated KSS in parenthesis)

Time	***One Variable***	***Two Variables***	***Three Variables***
t0	52.941 ThetaEAxisD (52.941) 44.118 RH850 (44.118) 35.294 D850 (35.294) 32.353 WeekAnt (32.353) 26.471 Lat (26.471)	55.882 D850, WeekAnt (47.059)	67.647 D850, RH700, WeekAnt (61.765) 67.647 D850, RH850, VV1000 (61.765)
t-3	52.941 ThickDiffWF (50.0) 44.118 ThetaEAxisD (44.118) 38.235 MidShearDir (38.235) 35.294 SoilM (35.294) 32.353 WeekAnt (32.353)	52.941 ThetaEAxisD, WeekAnt (50.0) 52.941 Pwat%,ThickDiffWF (38.235) 52.941 WCD, ThetaEAxisD (52.941) 52.941 MidShearSpd, ThickDiffWF (47.059) 52.941 LowShearDir, WeekAnt (50.0) 52.941 D500, ThickDiffWF (44.118)	67.647 VV850, ThetaEAxisD, WeekAnt (61.765)
t-6	52.941 Runoff (52.941) 38.235 MoistAv (35.294) 35.294 SoilM (35.2954) 32.353 WeekAnt (32.353) 29.412 WCD (29.412)	55.882 MBEDir, Runoff (52.941)	61.765 WCD, ThetaeFlood, WeekAnt (50.0)

The latitude of the events also proved to be one of the more significant differences, with flood events more often farther north than watch events (Figure 39). This may suggest that some portions of the CWA may contain more false alarms or more unanticipated floods than others. In general, flash flood watches are issued for a large portion of the CWA. To reduce these areas to a size comparable to those of the flash flood dataset, the county reporting the highest precipitation total was used to represent each watch case. These locations selected for the flash flood watches may be biased toward those areas of the CWA more prone to heavy rainfall, such as the southern half of the CWA. Precipitation totals would be expected to be higher in the southern portions of the BGM CWA for events with a southerly wind component due to the local topography, which causes downsloping downstream in the CWA.

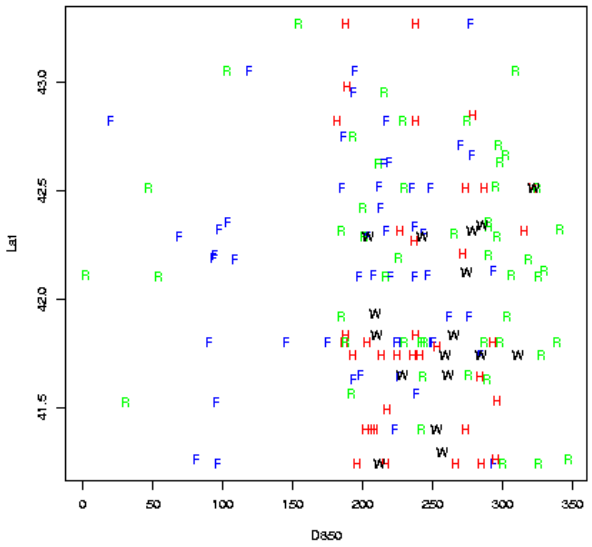

Figure 39. Latitude (degrees) and 850 hPa wind direction (degrees)
F=flood, H =heavy, W= watch, R=random\

At t-3, thickness diffluence (smaller magnitudes for watches) and 850-hPa θ_e axis distance (further to the east for watches) took on greater significance. Other significant parameters at this time included mid-level directional wind shear (almost

always veering with height for watches), soil moisture content, and weekly antecedent precipitation. The combination of 850-hPa vertical velocity (larger for watches), 850-hPa θ_e axis distance, and weekly antecedent precipitation improved the forecasting skill. At t-6, the larger antecedent soil moisture and precipitation for floods take on greater importance. The most capable predictor was runoff at the backtracked location (Figure 40). Although little to no runoff was common for both sets of events, the largest values of runoff were more common for the flood events than for the watch events. This suggests that flash flooding is more likely when heavy precipitation has occurred upstream, with reference to the 850 hPa winds. In addition to larger short-term and long-term rainfall, warm cloud depth helps to distinguish floods from watch events. The watch events typically had a larger warm cloud depth than the floods. The combination of warm cloud depth, θ_e at the site of the flood (slightly higher for watches), and weekly antecedent precipitation improved the skill somewhat; however, the cross validation suggests that this combination is suspect.

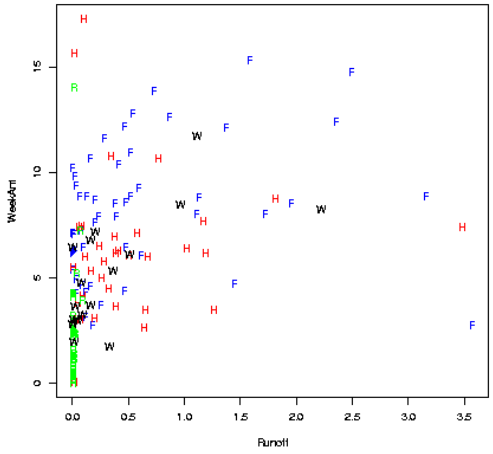

Figure 40. Surface Runoff (kg/m^2) and Weekly Antecedent Precipitation (cm)

For the convective events, the antecedent soil condition remained significant, particularly soil moisture and weekly antecedent precipitation. At t0, 850 hPa RH and

850 hPa wind direction were useful discriminators. The distance to the θ_e axis was significant for both t0 and t-3.

Discriminant Analysis Results - Flash Floods vs. Random Events

The greatest differences between the flash floods and the random climatology were generally in the antecedent precipitation and atmospheric moisture (Table 7; Figures 41- 43). As one might expect, the ground and the atmosphere proved to be significantly more moist than normal during flood events. The single best discriminator at all three time periods was weekly antecedent precipitation. A relatively high KSS for the monthly antecedent precipitation suggests that flash floods events tend to occur during abnormally wet periods. (Note: the same values were used for weekly antecedent precipitation for all three time periods, and likewise for monthly antecedent precipitation.) The measures of atmospheric moisture differing the most included precipitable water as a percentage of normal, mean 1000-500 hPa relative humidity, and 500-hPa relative humidity. The K-index also proved effective at discriminating between the two datasets. Great skill was attained through several

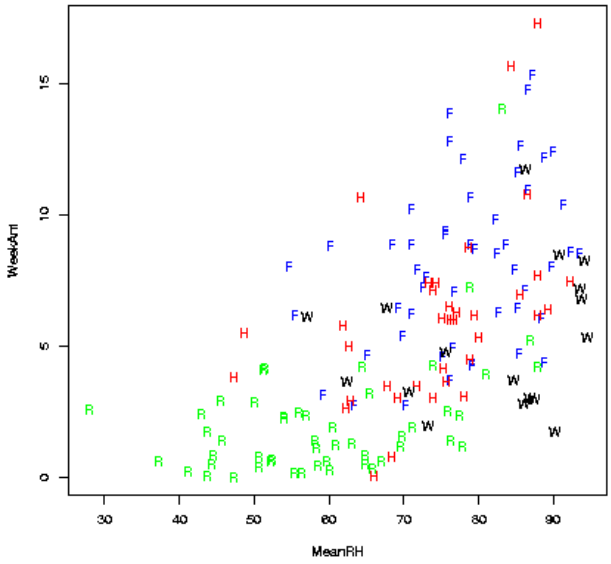

Figure 41. Weekly antecedent precipitation (cm) and mean 1000-500 hPa relative humidity (%)

Table 7. Flood/random discriminant analysis results, all cases
(cross validated KSS in parenthesis)

Time	***One Variable***	***Two Variables***	***Three Variables***
t0	72.549 WeekAnt (72.549) 60.784 Pwat% (60.784) 60.784 MeanRH (60.784) 60.784 RH500 (60.784) 58.824 Kind (56.863)	88.235 Td850, WeekAnt (86.275)	92.157 Pwat%, WeekAnt, SoilM (92.157) 92.157 Pwat%, WeekAnt, MoistAv (92.157) 92.157 Kind, WeekAnt, SoilM (90.196) 92.157 Kind, Pwat%, WeekAnt (90.196) 92.157 LI1000500, Pwat%, WeekAnt (92.157)
t-3	72.549 WeekAnt (72.549) 54.902 MonthAnt (54.902) 54.902 Kind (54.902) 52.941 MeanRH (52.941) 49.020 Pwat% (47.059)	86.275 Td850, WeekAnt (86.275) 86.275 Tdsfc, WeekAnt (82.353)	92.157 LI1000500, Pwat%, WeekAnt (88.235) 92.157 Td850, WeekAnt, SoilM (90.196) 92.157 Rhsfc, Kind, WeekAnt (92.157)
t-6	72.549 WeekAnt (72.549) 54.902 MonthAnt (54.902) 52.941 Kind (52.941) 49.020 Pwat% (49.020) 49.020 Tdsfc (49.020)	86.275 Td850, WeekAnt (84.314) 86.275 Tdsfc, WeekAnt (88.235)	96.078 MidShearSpd, LI1000500, WeekAnt (92.157)

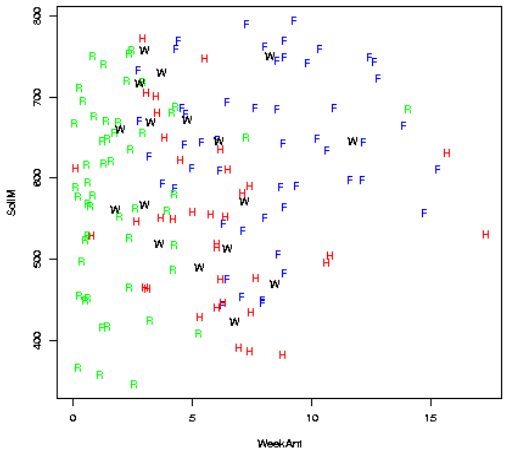

Figure 42. Weekly antecedent precipitation (cm) and soil moisture (kg/m^2)

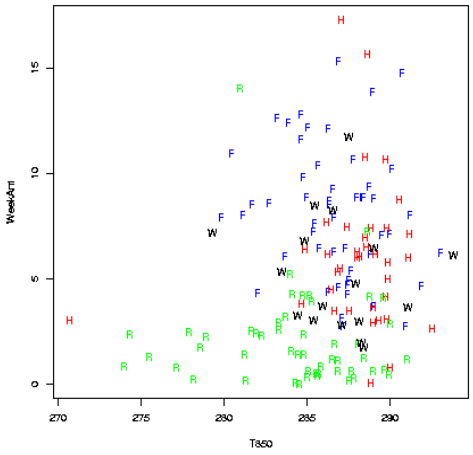

Figure 43. 850 hPa dewpoint temperature (Kelvins) and Weekly Antecedent Precipitation (cm)

combinations of three variables. Each of these combinations included weekly antecedent precipitation and precipitable water, along with either soil moisture, moisture availability, or lifted index, to attain a cross-validated skill of 92.157. The results at t0 are very similar to those at earlier time periods.

A concern with this result is that the weekly antecedent precipitation, soil moisture, and moisture availability are highly correlated with each other. Future work will address this by removing two of these parameters from the dataset.

Composite Maps

Daily composite maps of each group of events were plotted using NCEP/NCAR Reanalysis data (NOAA, 2005; Kalnay et al., 2005) to put the numerical results outlined above into a context more applicable to the real-time forecasting applications that will be the result of this work. Separate composite plots were made of May/September/October (MSO) and June/July/August (JJA) events for the flood, heavy, and watch cases. The composite maps were plotted to visualize the mean fields of each dataset. However, they do not reflect the variability within each dataset, nor do they reveal whether a subset of events in two different datasets may be similar. One other limitation is that the web application used to generate these composite maps limits the sample size to twenty. These limits on the compositing process should be kept in mind as the composite results are described below.

June/July/August Composites

The differences between the flood and heavy datasets were greatest in the JJA composites. In these plots, the flood events featured two distinguishing characteristics from the heavy events: their 1000-500 hPa moisture fields and the strength of mid-level (700 and 850 hPa) winds over the Great Lakes. First, the flood composites had relative humidities from 5%-10% higher over New York and northeast Pennsylvania in the 1000-500 hPa layer. This trend is reflected in the discriminant analysis results, where relative humidities at 850, 700, and 500 hPa were found to be significant predictors. At 1000 hPa, the distinction between the two scenarios was the location of the maximum relative humidity (Figure 44). For the flood events, the peak RH of 90%-95% was centered on the CWA. For the heavy events, the CWA was located in a broad area of 85%-90% RH, while the maximum was located in southwestern Ohio and eastern Indiana. The disparity in relative humidity was greatest at the 500 hPa level, where the flood composite had a value of 52.5%-55% over the CWA, while the

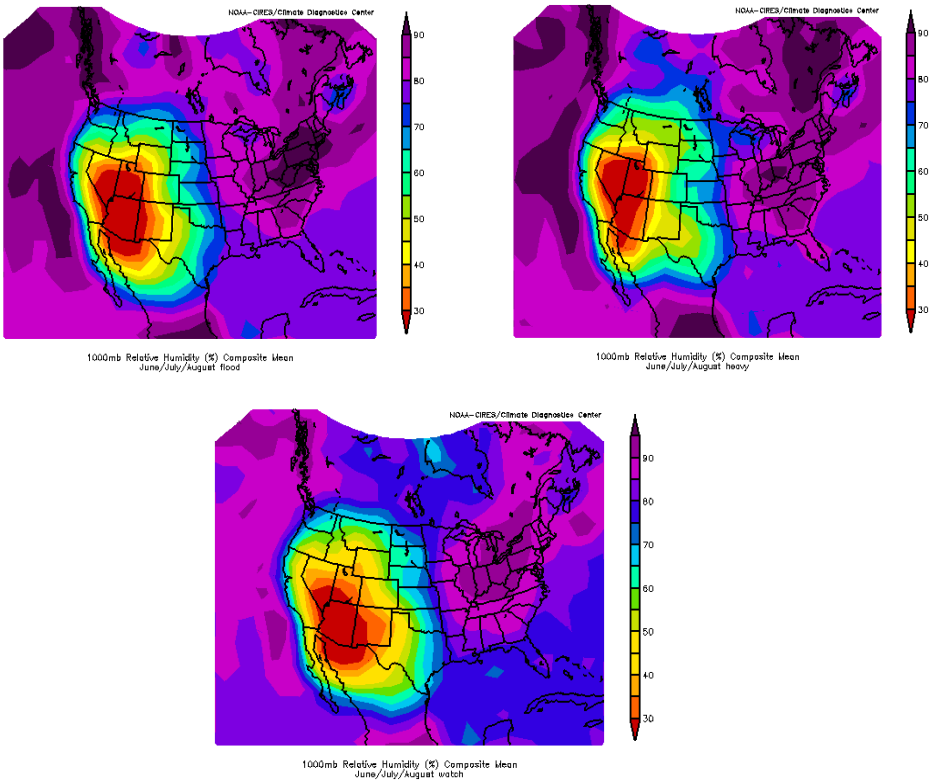

Figure 44. JJA 1000 hPa relative humidity (%)
(upper left - flood, upper right - heavy, bottom - watch)

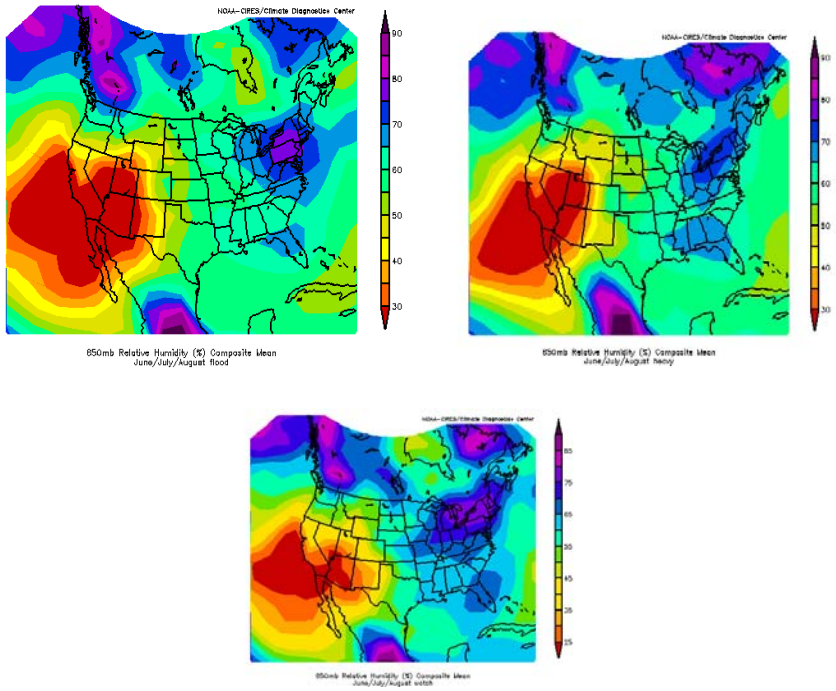

Figure 45. JJA 850 hPa relative humidity (%)

heavy composite had a local value of 40%-42.5% (Figure 45). The CWA was near the center of the peak relative humidity at 500 hPa in both the flood and heavy composites. In contrast, the relative humidity fields for the watch events differ from both the flood and heavy events in that the maxima are tilted through the lower troposphere. In addition, the areas of high relative humidity cover a much broader area in the watch composites than in the flood and heavy composites, particularly from 1000 hPa to 700 hPa. At 1000 hPa, the relative humidity for most of the U.S. east of the Mississippi exceeds 85%, with a large area including the Ohio Valley and the Great Lakes above 90%. At 850 hPa and 700 hPa, the watch relative humidities peak over the CWA, with higher values than both the flood and heavy composites (Figures 46, 47). The peak relative humidity at 500 hPa is located over New England, and the BGM CWA is located in a gradient from 45%-52.55%. Although the values of relative humidity throughout the lower to middle troposphere for the watch composites are similar to those of the flood and heavy composites, the axis of greatest moisture is tilted from southwest to northeast with height. In contrast, the flood composite and (to a lesser extent) the heavy composite feature a peak in the relative humidity field centered above the CWA throughout most of the lower troposphere.

In the precipitable water field, all three composite maps contained a minimum near the West Virginia/Kentucky/Virginia border and a ridge of high precipitable water along the Atlantic coast. However, the heavy and watch composites also contain a ridge stretching through the Ohio valley, just west of the Appalachian Mountains. The precipitable water anomaly maps reflect this difference (Figure 48). In the flood composite, abnormally high values of precipitable water are concentrated over southern New York, eastern Pennsylvania, New Jersey, and a neighboring section of the Atlantic Ocean. In the heavy composite, above-normal precipitable water values extend from the lower Mississippi valley up through the Ohio Valley and peak

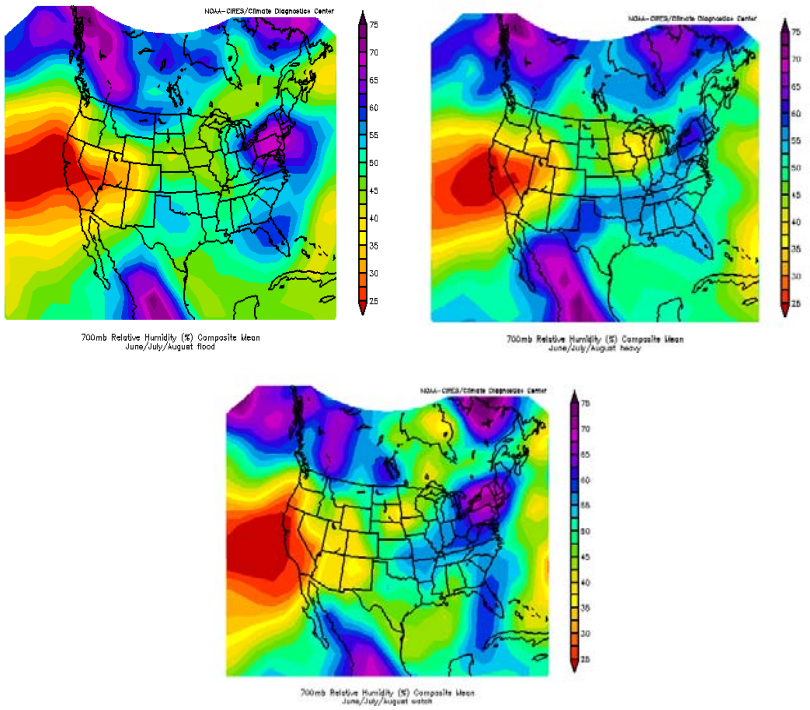

Figure 46. JJA 700 hPa relative humidity (%)

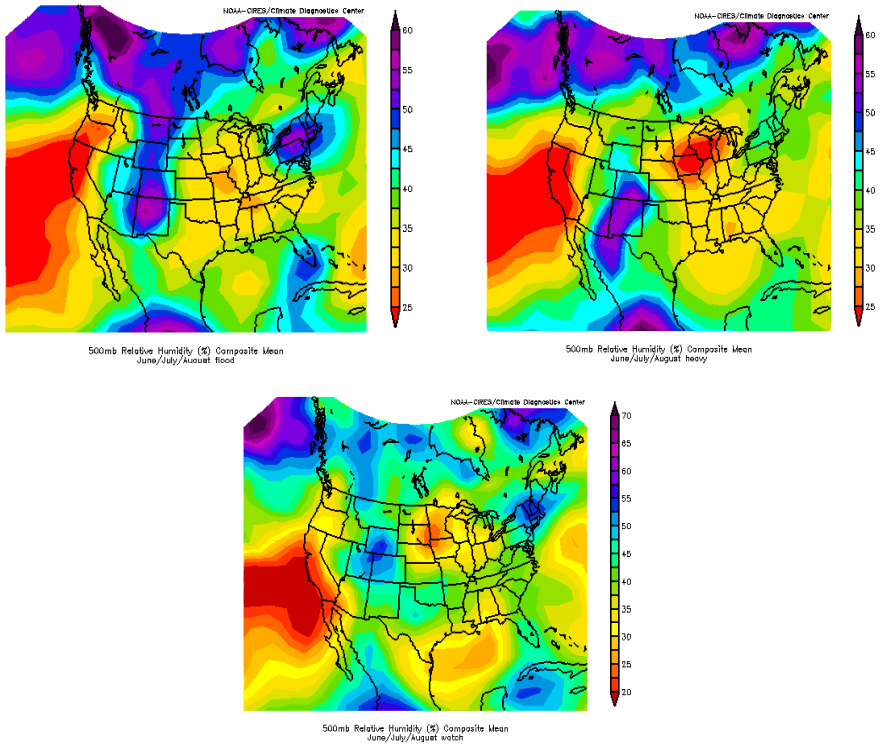

Figure 47. JJA 500 hPa relative humidity (%)

over New York. The swath of above-normal precipitable water is even larger for the watch events. The differences among precipitable water anomaly maps suggest a different moisture trajectory for the low-level inflow for the two types of events. It appears that the characteristic of the moisture field separating the floods from the non-flood events is the degree to which the moisture is focused. In the flood events, the local RH maxima are aligned throughout the 1000-500 hPa layer, concentrating the moisture over the CWA. In the two non-flood composites, the local RH maxima are tilted through the 1000-500 hPa layer, and the concentrations of high moisture are spread over a larger area. This observation suggests that flood events achieve a greater precipitation efficiency than non-events through the moister environment, which reduces the entrainment of dry air. This hypothesis may be tested in a future modeling study.

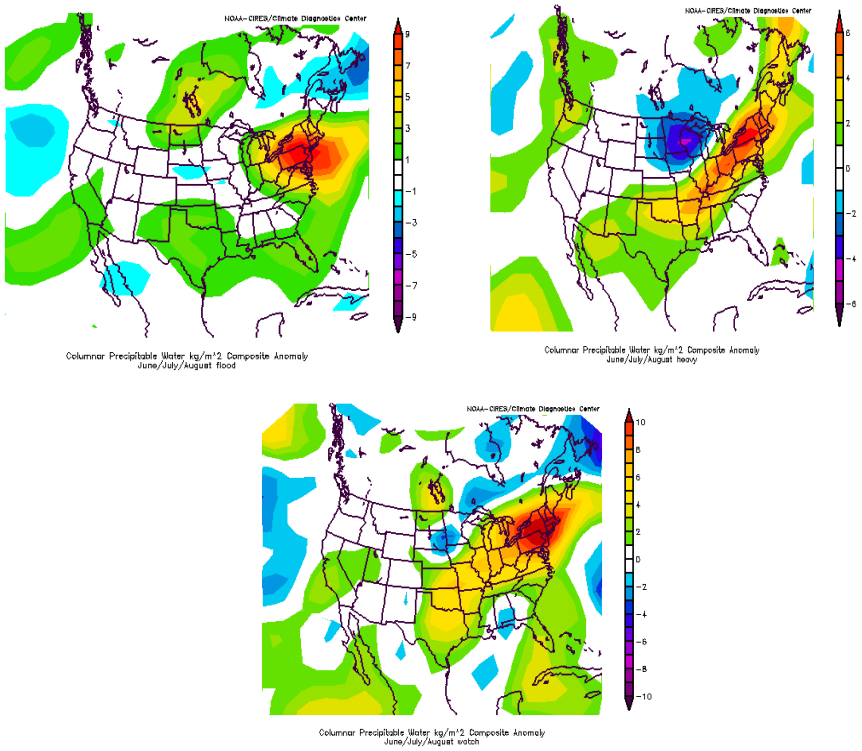

Figure 48. JJA Precipitable water (% normal)

The wind fields, particularly throughout the lower to middle troposphere, differ among the three datasets as well. This is supported by the discriminant analysis, as both the 850 hPa wind direction and storm motion direction were found to be good discriminators among the datasets. At 1000 hPa, the flood composite has very weak (<2 m/s) winds over the CWA (Figure 49). The wind direction is south-southeasterly, but given the small magnitude and the variable wind directions in the area, there does not appear to be a strong preference for this direction. In the heavy composite, the CWA is located in the left entrance region of a surface wind maximum, which is located over Newfoundland. Winds are southwesterly at 2-3.5 m/s. In the watch composite, winds are also southwesterly with speeds up to 3 m/s in the southern and eastern portions of the CWA. Both the flood and watch composites contain a maximum in 1000 hPa wind speed off the North Carolina coast, with a southerly direction. At 850 hPa, the flood composite contains a wind speed minimum to the northwest of the CWA, with westerly winds of 2 to 4 m/s across the CWA (Figure 50). The 850 hPa winds are still westerly but stronger across the CWA in the heavy composite, with speeds of approximately 6 m/s. The watch composite features aspects of both these composites. It contains the wind speed minimum to the northwest of the CWA, but stronger winds directly over the CWA (speeds of 6 to 9 m/s). The CWA is in the left entrance region of a jet located in the Atlantic Ocean east of Cape Cod. At 700 hPa and 500 hPa, the differences among the three composites resemble those at 850 hPa (Figure 51; 500 hPa winds not shown). The flood composite contains a minimum in wind speed over the Great Lakes with weaker winds over the CWA than the other two composites. The heavy composite has faster winds than the flood composite and no minimum over the Great Lakes, with a jet over Newfoundland. The watch composite has faster local winds than the other two composites, leading into a jet southeast of Nova Scotia. At upper levels (e.g. 300 and 250 hPa), all three

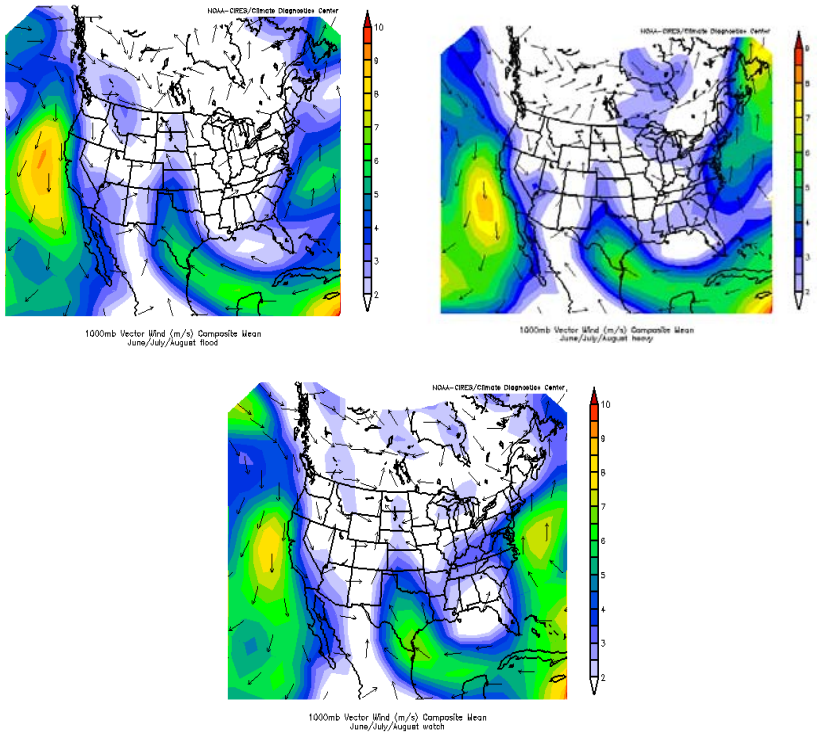

Figure 49. JJA 1000 hPa winds (m/s)

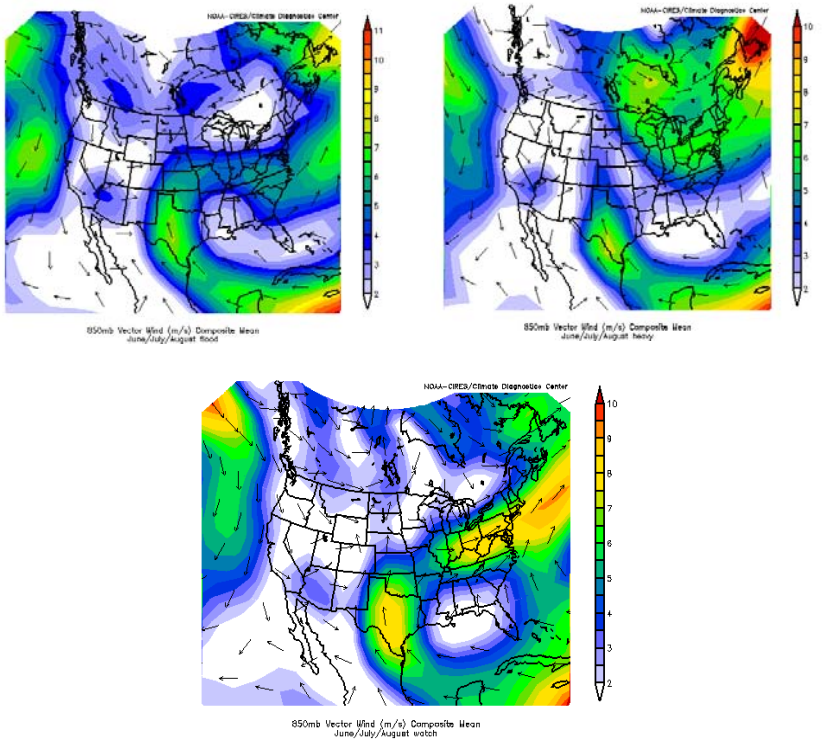

Figure 50. JJA 850 hPa winds (m/s)

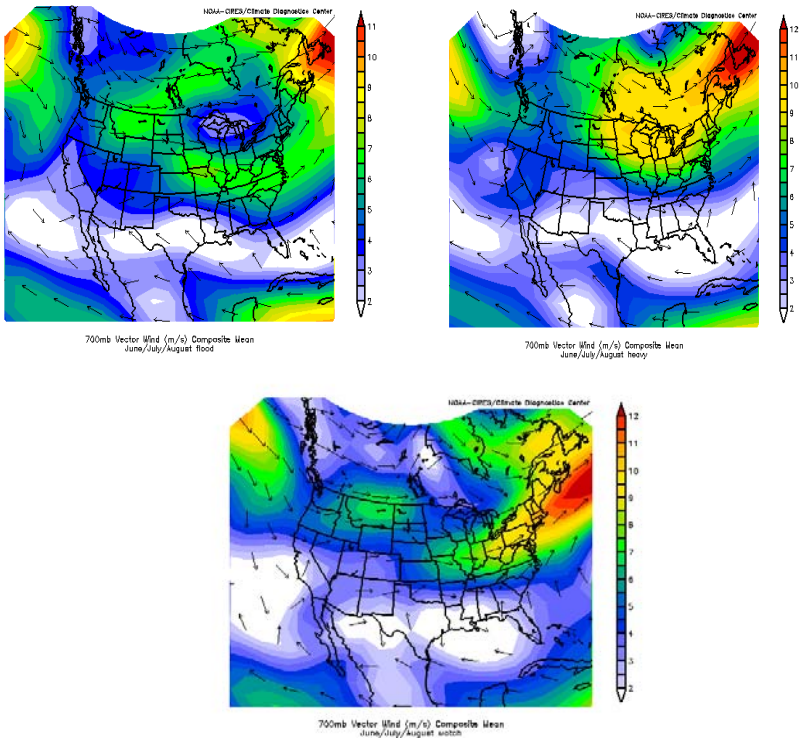

Figure 51. JJA 700 hPa winds (m/s)

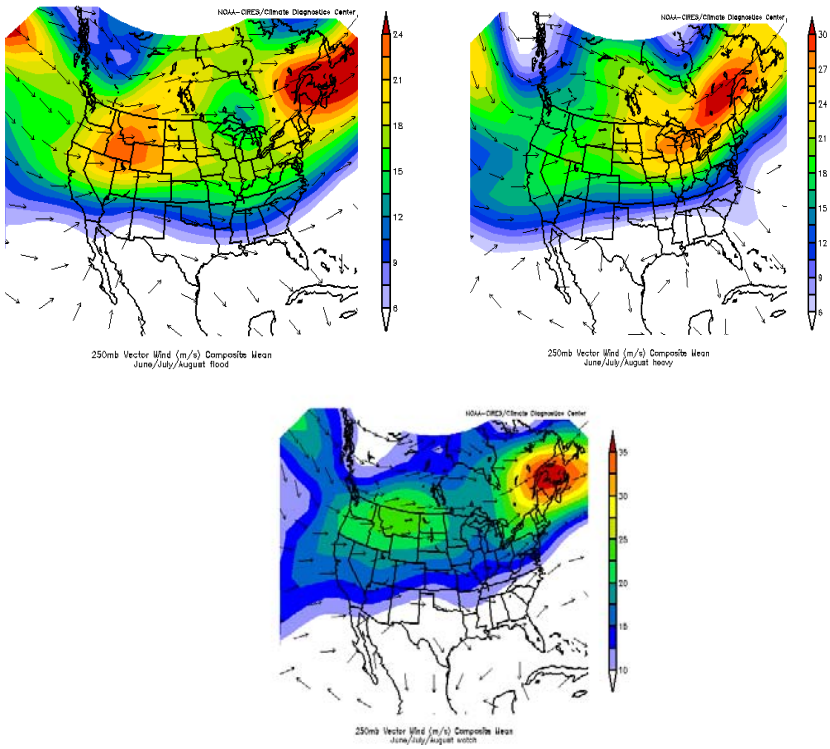

Figure 52. JJA 250 hPa winds (m/s)

composites contain jets over the Canadian eastern seaboard, putting the CWA in the divergent right entrance quadrant, with slight differences among the composites (Figure 52). The wind speed minimum over the Great Lakes from the lower levels persists in the flood composite and appears as a local minimum in the watch composite, but this feature is not present in the heavy composite. The jet in the heavy composite is much closer to the CWA than in the flood composite. Although the jet streak in the watch composite is located in a similar location to the flood composite, the watch composite's jet streak is nearly 10 m/s faster. The general tendency for the flood wind composites' winds to be slower in the lower to middle layer of the troposphere suggests that flooding is more likely with slower storm motion and lower shear values throughout this layer. In contrast, the upper level winds appear to be similar among all three datasets in that they favor divergence aloft.

The sea level pressure maps suggest differing synoptic situations for the three composites (Figure 53). The flood composite map has a local minimum pressure just to the west of the CWA, and a trough at the northern edge of the map north of northeastern Canada. The heavy composite contains a low east of the Hudson Bay, with a trough extending through the St. Lawrence River valley and along the eastern Great Lakes into eastern Indiana. The watch composite contains features of both the flood and heavy composites, namely a low between Lakes Michigan and Erie and a trough north of northeastern Canada extending into the St. Lawrence valley. Height maps (not shown) through the lower troposphere contain a weak trough over the eastern U.S. but neither a trough nor a ridge in the Hudson Bay region. The heavy and flood maps both contain similar troughs – the trough in the watch composite is farther west than in the heavy composite – but in both of these cases, the troughs extend north to the Hudson Bay region, where they are most prominent.

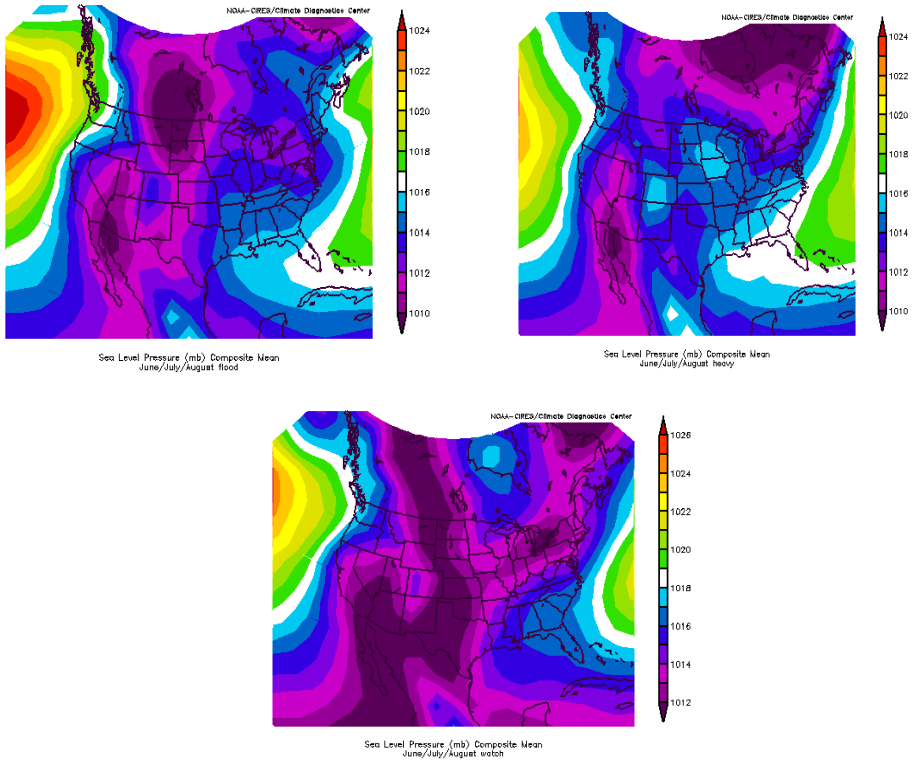

Figure 53. JJA Sea level Pressure (hPa)

May/September/October Composites

In general, the cold season composites are much similar to each other than the warm season composites. Because these cold season events tend to be largely non-convective, this may suggest that these non-convective events may rely more on antecedent soil moisture or some other non-meteorological factor. More research is needed to support this supposition. Neither the moisture fields nor the wind fields display much difference, particularly between the flood and heavy composites. These two datasets appear to differ in their sea level pressure fields, which suggests that the forcing for the events may be occurring on different scales. The watch composites display a decidedly different pattern than the flood and heavy composites. These composites are presented with a caveat: one must consider the smaller sample size when analyzing these results (flood=17, heavy=13, watch=5).

The relative humidity magnitudes and spatial distributions are very similar for the flood and heavy composites from 1000 hPa through 500 hPa (Figures 54-57). In both scenarios, the CWA is in the center of a very moist region of the northeastern U.S. and southern Canada at 1000 hPa and near the highest relative humidities at 850 hPa and 700 hPa. At 500 hPa, the peak relative humidities are located to the northwest (flood) and northeast (heavy) of the CWA, and the CWA lies in a gradient increasing in these directions. The similarities in the relative humidity fields are reflected in the precipitable water fields – the flood and heavy composites are similar in magnitude and shape. The watch composites, however, paint a slightly different picture. Throughout the 1000-700 hPa layer, the CWA lies at the northwestern corner of the region of peak relative humidity, and the relative humidity is approximately 5%-10% higher than the other two scenarios. At 500 hPa, the relative humidity maximum is centered on the NY/PA border, in the center of the CWA. Consequently,

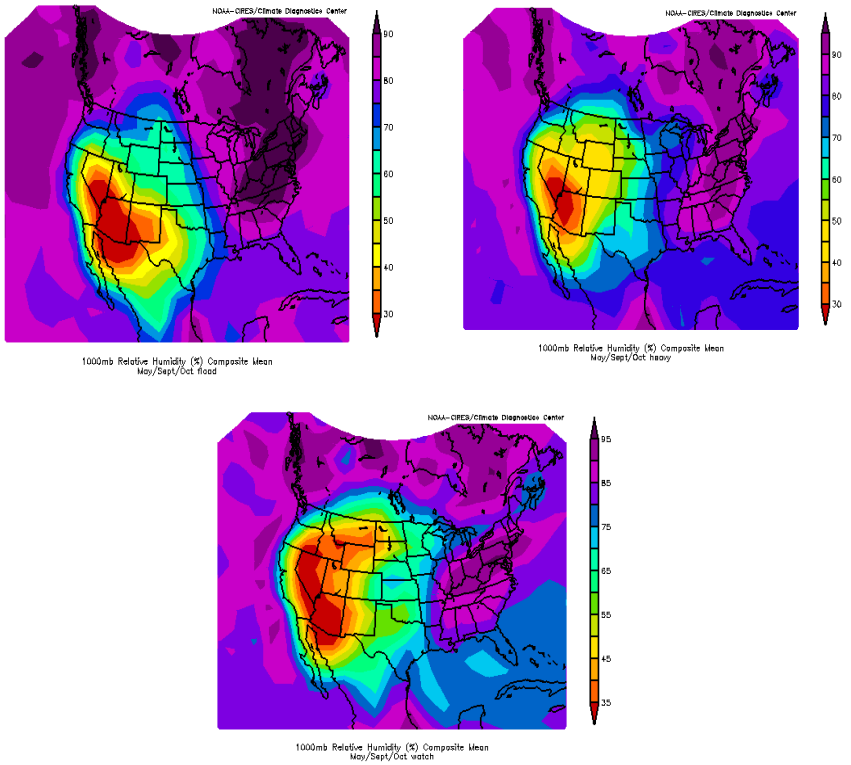

Figure 54. MSO 1000 hPa relative humidity (%)

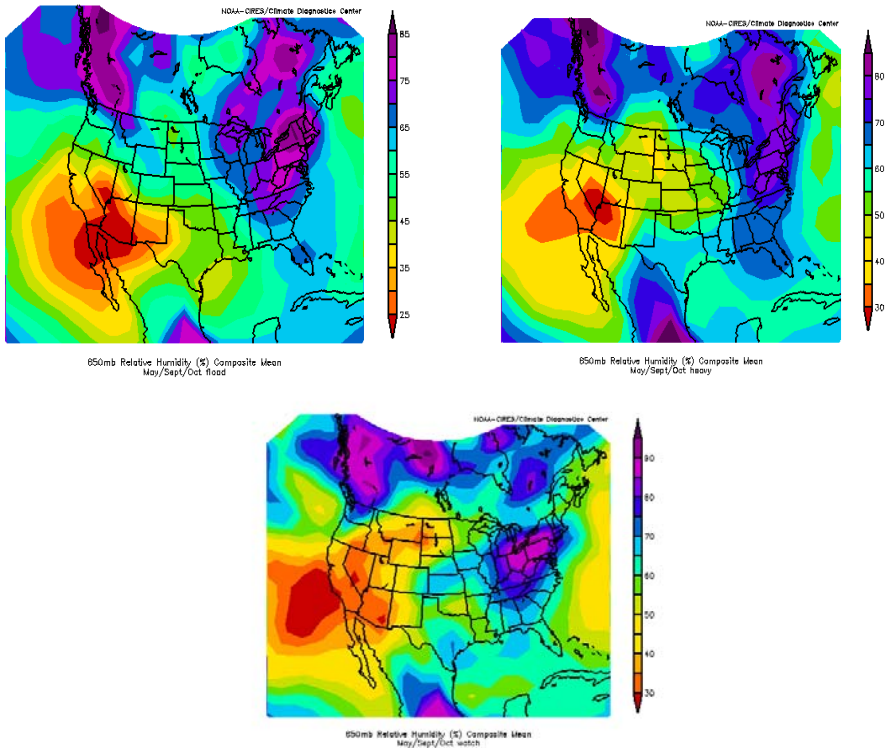

Figure 55. MSO 850 hPa relative humidity (%)

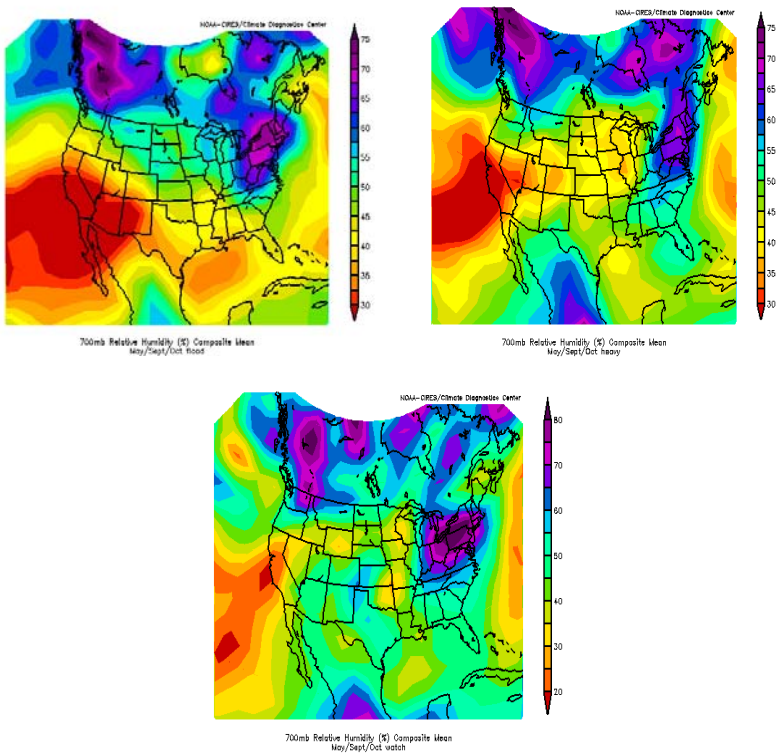

Figure 56. MSO 700 hPa relative humidity (%)

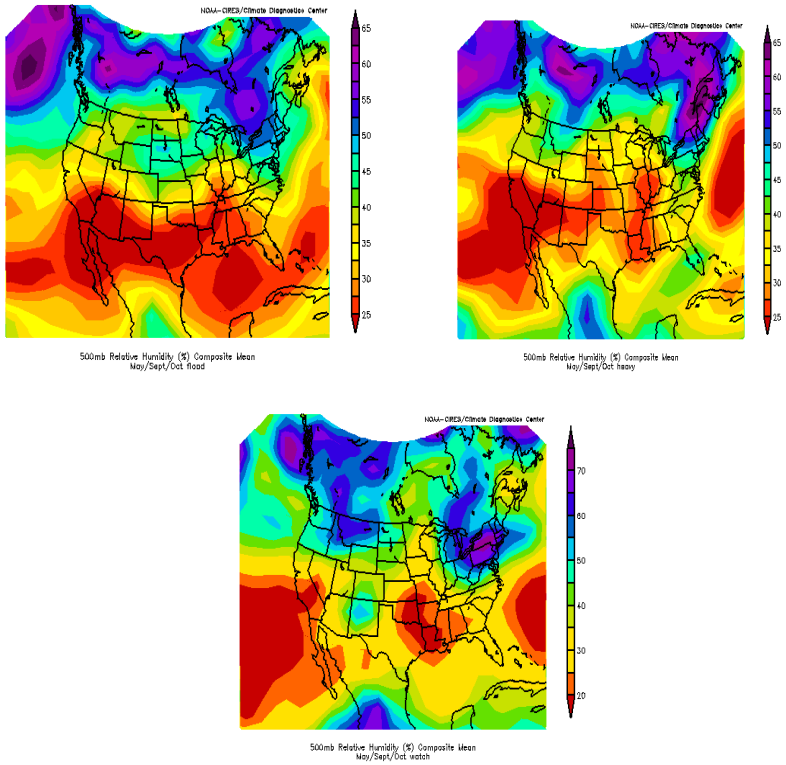

Figure 57. MSO 500 hPa relative humidity (%)

relative humidities are approximately 20% higher for the watch composites than for the other two scenarios. The watch precipitable water anomaly composite (not shown) is larger in magnitude than the other two composites and focuses the greatest anomalies south of the CWA, rather than to the east, as in the flood and heavy composites. Some of these differences may be attributed to the sample sizes – the watch composite is comprised of only five members.

The wind composites are also quite similar to each other, especially for the flood and heavy cases (Figures 58-61). All three composites have a relatively weak westerly wind at 1000 mb with a southerly 1000 mb maximum over the Atlantic Ocean east of New Jersey and the Delmarva Peninsula. The composites are also similar at the top of the troposphere, with a strong (> 30 m/s) jet over Quebec at 200

hPa. Winds throughout the rest of the troposphere tend to share the same southwesterly direction, except at 850 hPa, where the flood and heavy composites contain southwesterly winds, while the watch composite is westerly. However, the locations of peak wind speeds through the lower and middle troposphere differ. The flood and heavy composites include a 700 hPa jet (>12 m/s) over western New England and eastern New York, and a 850 hPa jet (9 to 10 m/s) over southern New England. This puts the CWA in the convergent right entrance region of the jet.

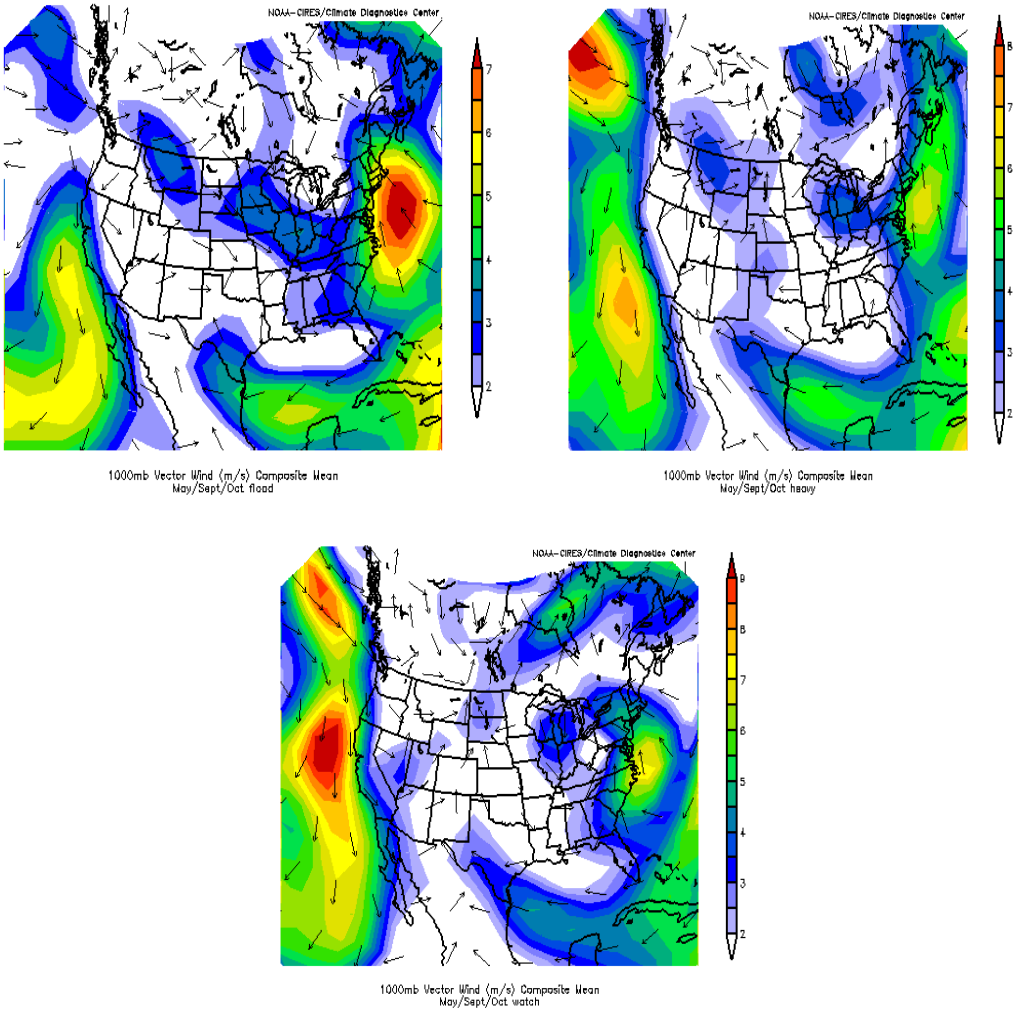

Figure 58. MSO 1000 hPa winds (m/s)

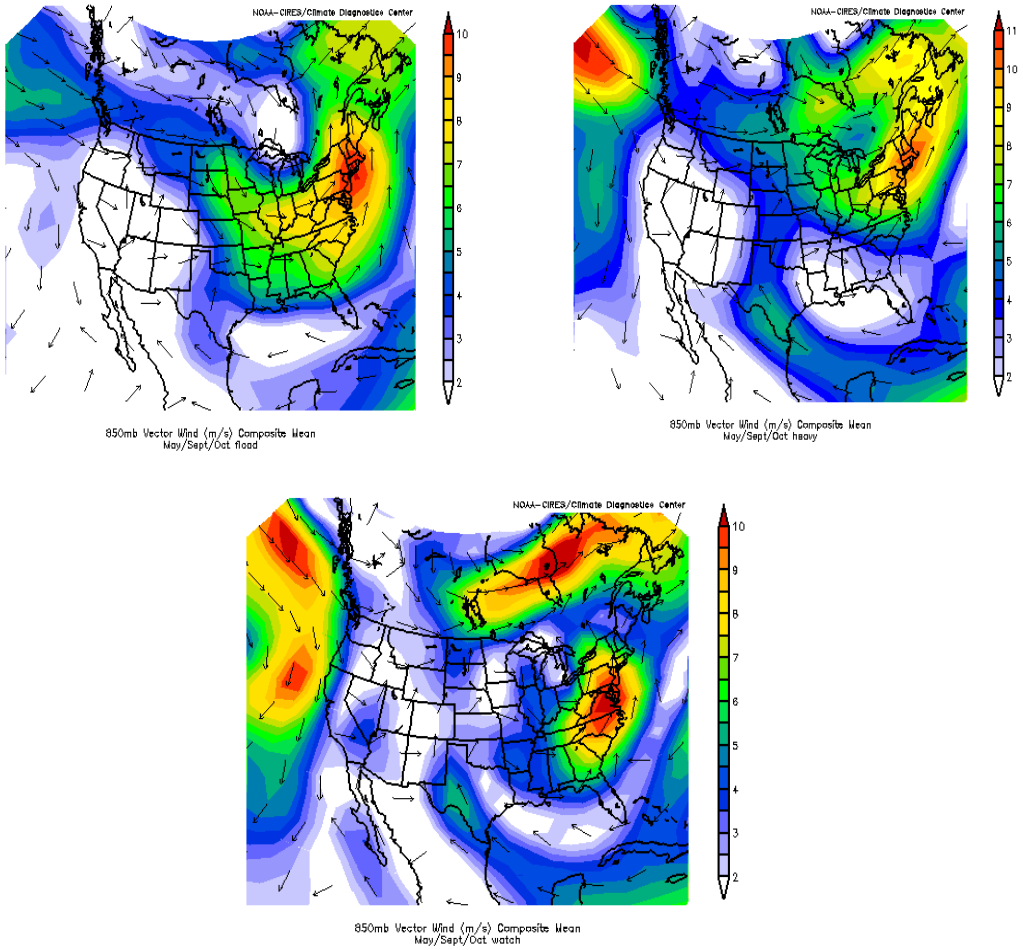

Figure 59. MSO 850 hPa winds (m/s)

Their wind fields differ only at 500 hPa, where the heavy jet streak (20 m/s) extends from central New York to northern Quebec, while the flood jet streak (also 20 m/s) is confined to northern Quebec. The watch composite features different jet streak locations. In the 850-500 hPa layer, maximum winds are located south of the CWA, in the Virginia/North Carolina vicinity. This places the CWA in the divergent left exit quadrant of the jet streak. Thus, the main difference among the wind fields is that the flood and heavy events put the CWA in a convergent region in the 850-700 hPa, while the watch composites exhibit divergence in this layer.

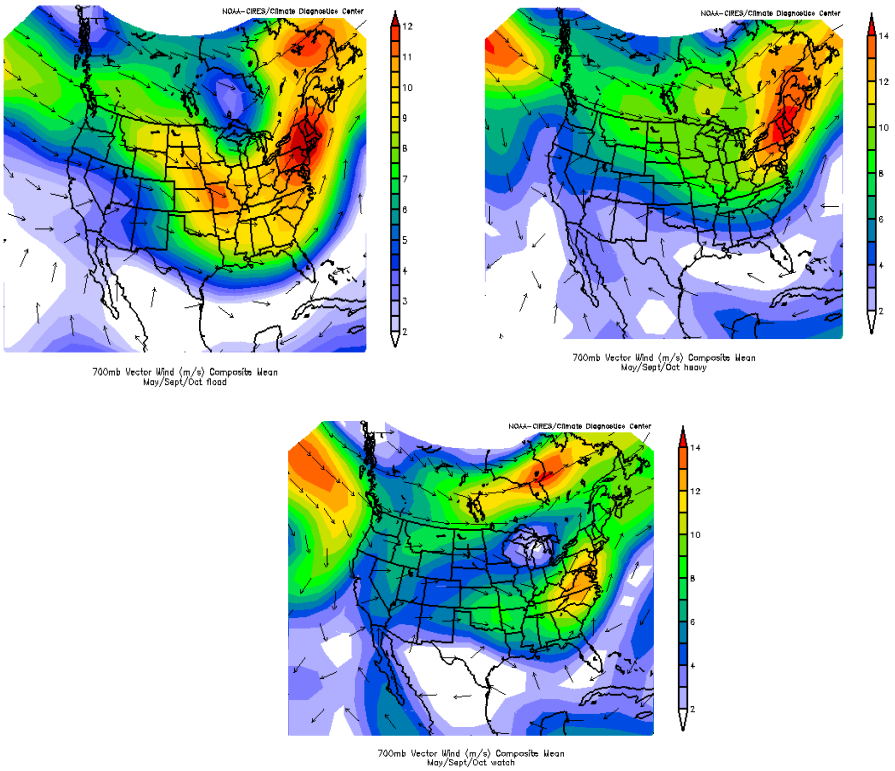

Figure 60. MSO 700 hPa winds (m/s)

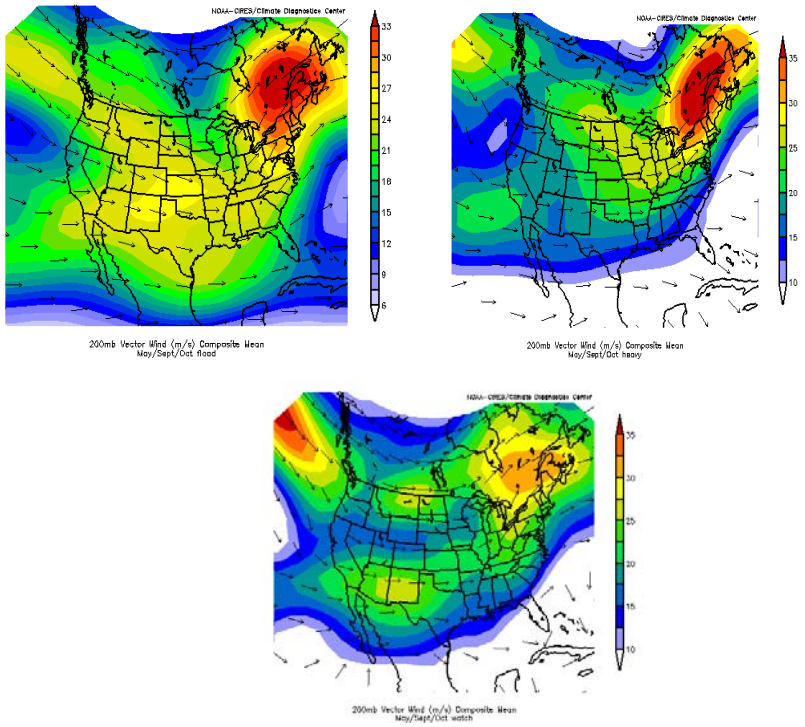

Figure 61. MSO 200 hPa winds (m/s)

In contrast to the other parameters, the sea level pressure field is most similar between the flood and watch composites, but differs for the heavy composite (Figure 62). All three maps have a trough in extreme northeastern Canada. However, both the flood and watch composites display a distinct low pressure center over the Great Lakes region, while the heavy composite doesn't show a cut-off surface low, but does contain a trough though the St. Lawrence valley into the Ohio valley. Thus, with a nearby low pressure center occurring frequently enough to appear in the composite, the flood and watch events may have been dominated by synoptic-scale forcing around this low, while the forcing for the heavy events may have been more frequently along mesoscale features such as a cold front (i.e. the trough axis) or a low-level convergence zone. Because the variability of the events comprising each composite map cannot be determined, more work is needed to support this hypothesis.

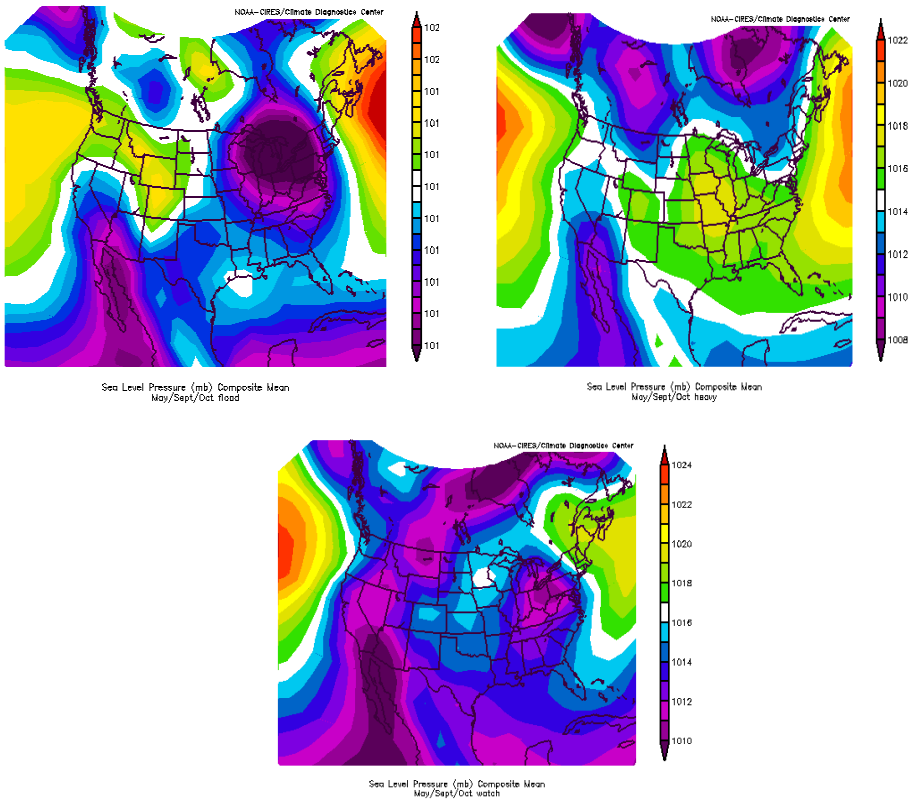

Figure 62. MSO Sea level Pressure (hPa)

Another potential distinguishing factor between the flood and heavy events may have been soil moisture due to antecedent precipitation. The NARR soil moisture data and cooperative station antecedent precipitation observations show that most heavy MSO events had lower antecedent soil moisture than the flood events. To a lesser extent, this is also true for the flood events in comparison to the watch events. This result suggests that hydrology may be more important than meteorology in determining the flooding potential of these types of events. Future work will examine this possibility.

In summary, the distinctions among the cold-season events appears to be that while the watch events had a similar synoptic situation - but with even more moisture throughout the lower to middle troposphere – in comparison to the flood events, the lower level divergence present in the watch cases may have prevented the moisture from concentrating in a confined area and producing a flood. The main distinctions between the heavy and flood events include the soil condition prior to the event (generally drier for the heavy events), and the difference in sea level pressure composites, which may have reflect different forcing mechanisms for the majority of each type of event.

CHAPTER FOUR

DISCUSSION

The results of this study demonstrate that antecedent precipitation and antecedent soil moisture are often the key distinguishing factor between a flash flood and a non-flood event. Other authors have suggested this result (e.g. Doswell et al., 1996), but the statistical significance of antecedent soil moisture has not been quantified in the published literature. Several cases in this study generated heavy precipitation with moist antecedent soil conditions, yet did not produce flash flooding. This suggests that other factors play a role in determining which precipitation events cause flash flooding.

Through the combination of quantitative (discriminant analysis and cross-validation) and qualitative (daily composite maps) analysis, this study has shown that the meteorological conditions of a given precipitation event can offer some clues as to whether it will produce flash flooding. The results substantiate some portions of the BGM flash flood checklist, while contradicting others. Before comparing the quantitative and qualitative results, the differences between the two data sets should be noted. The composite maps are daily composites constructed from the global reanalysis, which has a 2.5 degree, 6-hour resolution – more coarse in both time and space than the NARR (32-km, 3 hour). Thus, some parameters that appear to be significant in the discriminant analysis may not appear as prominently in the composite maps, and vice versa. In particular, the composite maps show the predominant synoptic conditions in place during the event days, while the discriminant analysis is considering primarily the NARR-derived local environment during the event itself. From a forecasting perspective, the composite analysis may be useful when issuing flash flood watches more than six hours in advance, while the

discriminant analysis may be more useful in the short-term forecasting of precipitation events.

Based on the quantitative and qualitative results, the flash flood checklist in use at NWS BGM prior to this thesis had both strengths and weaknesses. Some of the best aspects of this checklist included indicators of moisture, particularly relative humidity in the 1000-500 hPa layer and precipitable water as a percentage of normal. It should be noted that, based on the seasonal composites, these measures are better at distinguishing between the floods and non-floods in JJA than in MSO. In general, flood composites are moister throughout the depth of the 1000-500 hPa layer, resulting in larger deviations from normal precipitable water in the summer. In MSO, there appears to be little difference among the moisture fields of the three types of events, and the greatest lower to mid-tropospheric moisture values appear in the watch composites, rather than the flood composites. Although the precipitable water threshold of 150% holds true for many events, it should be noted that this condition is not necessary for flash flooding. At the same time, this threshold can be misleading, as many of the non-floods exceed 150% of normal as well.

One of the most misleading components of the BGM checklist was the criterion of a low-level jet (LLJ) of at least 10.28 m/s (20 knots). The NARR 850 hPa winds, used to represent the LLJ, exceeded this threshold in fewer than half of the cases. The flood composite also showed relatively light 850 hPa winds over and upstream of the BGM CWA. The rationale for expecting a strong LLJ is that a significant injection of moist low-level air is necessary to provide enough moisture to generate the relatively large amounts of precipitation needed for flash flooding. Instead, it appears that the extremely moist local environment over New York and Pennsylvania was the primary source of the precipitation in most cases, with some additional low-level moisture advected into the region by the weak 850 hPa winds.

Another significant finding related to the 850-hPa winds is that a southeasterly wind direction was almost exclusively associated with flash flooding in the southern half of the CWA. The topography in this region is dominated by the Pocono Mountains in Pennsylvania and the Catskill Mountains in New York, suggesting that orography plays a role in favoring these areas. For a southeasterly flow, this would be a region of upslope winds, which would support convection. In contrast, areas further north and west within the CWA would be areas of downsloping flow under this scenario, which would be less favorable for convection and, therefore, less favorable for flash flooding.

At mid levels (700 – 500 hPa), the observations agreed with the checklist's suggestion of lighter winds. The flood composite maps showed a prevalent minimum in wind speed upstream, over the Great Lakes region. Because this feature appeared much less prominently in the watch composites and not at all in the heavy composite, it may be a key synoptic scale indicator of flash flooding. Therefore, this feature should be emphasized to a greater extent in the revised version of the checklist. Interestingly, the mid-level winds do not emerge from the discriminant analysis as significant parameters. This is most likely due to the displacement of the wind speed minimum from the CWA. Another possibility is that on the spatial and temporal scale of the NARR, local winds at these levels during the storm are similar in the flood and non-flood cases.

Upper level winds also agreed with the checklist, and upper-level divergence in the right entrance region of the jet appears to be a key component of a significant precipitation event. However, since the flood, heavy, and watch composites place the upper-level jet in a similar region with a similar intensity, it should be noted that this feature alone is not sufficient for flash flooding to occur.

The checklist also suggests that slow storm motion is favorable for flash flooding. Both the storm motion parameter – a modified Corfidi vector generated from the NARR winds – and the composite maps showing relatively light winds through the 1000 hPa – 500 hPa layer support this idea. The storm motion direction also appeared to be a somewhat effective differentiator of floods from non-flood events. However, the checklist notes that fast storm motions may be present in scenarios where the cell training can occur, and several cases agree with this assertion.

In terms of the synoptic variables, thickness diffluence appeared to be a useful discriminator in several comparisons, yet the composite maps contained only hints of weak thickness diffluence, at most, for each dataset. This may be another case of a feature that appears over too small a spatial and temporal scale to appear prominently in the composites. In contrast, there is notable evidence that the patterns of 850 hPa θ_e differ for floods and non-flood events. Contradictory to the checklist, flash flooding appears to be less dependent on a strong θ_e ridge than the non-flood events, especially during meteorological summer (JJA). Streaming moisture from the southwest is evident in both the heavy and watch composites, while the flood composites tend to favor a more localized maxima in atmospheric moisture, and a preference for the Atlantic Ocean as a moisture source, rather than the Gulf of Mexico. This implies that flood events are less dependent on θ_e ridging as a means of bringing moist air from the Gulf region. Future work is needed to examine this hypothesis in greater detail.

In summary, this research has resulted in several suggestions for a new paradigm of flash flood forecasting. The first concern of forecasters should be the current soil moisture condition. Flash flooding is very infrequent when little rain has fallen in the last week, but much more common during wet periods. High concentrations of moisture in the region of the forecast area that persist for at least the day of the flood also appear to be significant for flash flooding. In the summer months

especially, a column of locally available, above-normal moisture from 1000 hPa to 500 hPa helps to increase the precipitation efficiency by reducing the amount of dry entrainment. In contrast, lower moisture values in the mid-troposphere (700-500 hPa) and a long trajectory of moisture from the Gulf coast appear to be unfavorable to flash flooding. Weak mid-level winds appear to favor flash flooding, especially when these winds are increasing from a minimum over the Great Lakes to a jet off the coast of the northeastern U.S. In the cooler months (May, September, and October), the presence of a nearby low pressure center appears to influential in focusing and sustaining the precipitation of flood events, while the convection appears to be more likely along a cold front or a squall line in the non-flood cases. Future work will explore the variability within these general trends, with the goal of identifying situations consistently associated with flash flooding. The key to flash flood forecasting is identifying those patterns in which the meteorological conditions affect whether or not flash flooding will occur, and describing those patterns. With this knowledge, forecasters can more accurately anticipate flash flood events and, just as importantly, recognize those situations where heavy precipitation is not as likely to induce flash flooding.

REFERENCES

Bohl, V. G., and N. W. Junker, 1987: Using Climatologically Favored Thickness to Local the Axis of Heaviest Rainfall. *National Weather Digest*. Vol.. 12, pp. 5-10.

Bosart, Lance F. and Frederick Sanders. 1981: The Johnstown Flood of July 1977: A Long-Lived Convective System. *Journal of the Atmospheric Sciences*: Vol. 38, No. 8, pp. 1616–1642.

Caracena, Fernando, Robert A. Maddox, L. Ray Hoxit and Charles F. Chappell. 1979: Mesoanalysis of the Big Thompson Storm. *Monthly Weather Review*: Vol. 107, No. 1, pp. 1–17.

Changnon, S. A., 1999: Record Flood-Producing Rainstorms of 17-18 July 1996 in the Chicago Metropolitan Area. Part III: Impacts and Responses to the Flash Flooding. *Journal of Applied Meteorology*, Vol. 38, pp. 273-280.

Corfidi, S.F., J.H, Meritt, and J.M. Fritsch, 1996: Predicting the Movement of Mesoscale Convective Complexes. *Weather and Forecasting*, Vol. 11, pp. 41-46.

Creutin, Jean-Dominique, and Marco Borga, 2003: Radar hydrology modifies the monitoring of flash-flood hazard. *Hydrological Processes*, Vol. 17, pp. 1453-1456.

De Michele, C. and G. Salvadori, 2002: On the derived flood frequency distribution: analytical formulation and the influence of antecedent soil moisture condition. *Journal of Hydrology*, Vol. 262, pp. 245-258.

Doswell, C. A., H. E. Brooks, and R. A. Maddox, 1996: Flash Flood Forecasting: An Ingredients-Based Methodology. *Weather and Forecasting*, Vol. 11, pp.560-581.

Funk, T. W., 1991: Forecasting Techniques Utilized by the Forecast Branch of the National Meteorological Center During a Major Convective Rainfall Event. *Weather and Forecasting*, Vol. 6, pp. 548-564.

Giordano, Louis A. and J. Michael Fritsch. 1991: Strong Tornadoes and Flash-Flood-Producing Rainstorms During the Warm Season in the Mid-Atlantic Region. *Weather and Forecasting*: Vol. 6, No. 4, pp. 437–455.

Harnack, Robert P., Kirk Apffel and Joseph R. Cermak III. 1999: Heavy Precipitation Events in New Jersey: Attendant Upper-Air Conditions. *Weather and Forecasting*: Vol. 14, No. 6, pp. 933–954.

Hirsch M. E., A.T. DeGaetano, and S. J. Colucci, 2002: Statistical Prediction of Seasonal East Coast Winter Storm Frequency. *Journal of Clim*ate,Vol.15, pp. 1101-1117.

Junker, N. W., R. S. Schneider,and S. L. Fauver, 1999: A Study of Heavy Rainfall Events during the Great Midwest Flood of 1993. *Weather and Forecasting,*Vol. 14, pp. 701-712.

Kalnay, E., M. et al., 1996: The NCEP/NCAR 40-Year Reanalysis Project. *Bulletin of the American Meteorological Society*, Vol. 77, pp. 437-472.

Konrad II, Charles E. 1997: Synoptic-Scale Features Associated with Warm Season Heavy Rainfall over the Interior Southeastern United States. *Weather and Forecasting*: Vol. 12, No. 3, pp. 557–571.

LaPenta, K. D., B. J. McNaught, S. J. Capriola, L. A. Giordano, C. D. Little, S. D. Hrebenach, G. M. Carter, M.D. Valverde, and D. S. Frey, 1995: The Challenge of Forecasting Heavy Rain and Flooding throughout the Eastern Region of the National Weather Service. Part I: Characteristics and Events. *Weather and Forecasting*, Vol. 10, pp. 78-90.

Maddox, Robert A., Lee R. Hoxit, Charles F. Chappell and Fernando Caracena. 1978: Comparison of Meteorological Aspects of the Big Thompson and Rapid City Flash Floods. *Monthly Weather Review*: Vol. 106, No. 3, pp. 375–389.

Maddox, R. A., C.F. Chappell, and L.R. Hoxit, 1979: Synoptic and Mesoscale Aspects of Flash Flood Events. *Bulletin of the American Meteorological Society*, Vol. 60, pp. 115-123.

Mesinger, F., G. DiMego, E. Kalnay, P. Shafran, W. Ebisuzaki, D. Jovic, J. Woollen, K. Mitchell, E. Rogers, M. Ek, Y. Fan, R. Grumbine, W. Higgens, H. Li, G. Manikin, D. Parrish and W. Shi, 2004: North American Regional Reanalysis. Preprints AMS 2004 Annual meeting, Seattle WA.

Moore, J. T., Glass, F. H., Graves, C. E., Rochette, S.t M., Singer, M. J., 2003: The Environment of Warm-Season Elevated Thunderstorms Associated with Heavy Rainfall over the Central United States. *Weather and Forecasting*, Vol. 18, pp. 861-878.

NOAA, 2005: *Daily Climate Composites*. Online resource. Boulder, Colorado, NOAA-CIRES Climate Diagnostics Center. <http://www.cdc.noaa.gov/Composites/Day/>.

NOAA, 1986-2003: *Storm Data*. Ashville, NC, NESDIS, National Climatic Data Center. Vol. 28-45.

Ogden, F.L., H.O. Sharif, S.U.S. Senarath, J.A. Smith, M.L. Baeck, and J.R. Richardson, 2000: Hydrologic analysis of the Fort Collins, Colorado, flash flood of 1997. *Journal of Hydrology*, Vol. 228, pp. 82-100.

Opitz, H. H., S.G. Summer, D.A.Wert, W.R. Snyder, R.J. Kane, R.H. Brady, P.M. Stokols, S.C. Kuhl, and G.M. Carter, 1995: The Challenge of Forecasting Heavy Rain and Flooding throughout the Eastern Region of the National Weather Service. Part II: Forecast Techniques and Applications. *Weather and Forecasting*, Vol. 10, pp. 91-104.

Randerson. Darrell, 1976: Meteorological Analysis for the Las Vegas, Nevada, Flood of 3 July 1975. *Monthly Weather Review*: Vol. 104, No. 6, pp. 719–727.

Schultz, Larry W. 1984: The Central Kansas Flash Floods of June 1981. *Bulletin of the American Meteorological Society*: Vol. 65, No. 3, pp. 228–234.

Showalter, A.K., 1953: A Stability Index for Thunderstorm Forecasting. *Bulletin of the American Meteorological Society*: Vol. 34, pp. 250–252.

Smith, James A., Mary Lynn Baeck, Julia E. Morrison and Paula Sturdevant-Rees. 2000: Catastrophic Rainfall and Flooding in Texas. *Journal of Hydrometeorology*: Vol. 1, No. 1, pp. 5–25.

Smith, James A., Mary Lynn Baeck, Julia E. Morrison, Paula Sturdevant-Rees, Daniel F. Turner-Gillespie and Paul D. Bates. 2002: The Regional Hydrology of Extreme Floods in an Urbanizing Drainage Basin. *Journal of Hydrometeorology*: Vol. 3, No. 3, pp. 267–282.

Weaver, John F., Eve Gruntfest and Glenn M. Levy. 2000: Two Floods in Fort Collins, Colorado: Learning from a Natural Disaster. *Bulletin of the American Meteorological Society*: Vol. 81, No. 10, pp. 2359–2366.

Wilks, D. S., 1995: *Statistical Methods in the Atmospheric Sciences.* San Diego, Academic Press., 465 pp.

Zhang, Da-Lin and J. Michael Fritsch. 1986: Numerical Simulation of the Meso-β Scale Structure and Evolution of the 1977 Johnstown Flood. Part I: Model Description and Verification. *Journal of the Atmospheric Sciences*: Vol. 43, No. 18, pp. 1913–1944.

Zhang, Da-Lin and J. Michael Fritsch. 1987: Numerical Simulation of the Meso-β Scale Structure and Evolution of the 1977 Johnstown Flood. Part II: Inertially Stable Warm-Core Vortex and the Mesoscale Convective Complex. *Journal of the Atmospheric Sciences*: Vol. 44, No. 18, pp. 2593–2612.